Linear Interaction Approximation for the Prediction of Noise Generated by Turbulence/Shock Interaction

S. J. Leib *
HX5, LLC, NASA Glenn Research Center, Cleveland, Ohio 44135

In this paper we review the basic development of Linear Interaction Approximation (LIA), a linear inviscid approach to study the interaction of weak turbulence with flow discontinuities, and implement a formulation to calculate the acoustic field due to the incidence of vortical and entropic disturbances on a planar shock. The work is motivated by the observance in nozzles with internal mixers and external plugs of a shock formed by local flow accelerations, even at sub-critical pressure ratios. Exhaust systems with internally mixed/externally plugged nozzles are currently under consideration for use in commercial supersonic aircraft and it is important to have an assessment of the impact of this shock on the noise radiated by these nozzles. Numerical results are presented for the fluctuating pressure emitted by (separate) incident single-wave vorticity and entropy modes and for incident isotropic fields of turbulence and entropy. Further applications of the formulation to the flow fields in internally mixed/externally plugged nozzles, and to the modification of mixing noise sources and the scattering of internally generated noise by the shock, are discussed as future work.

I. Introduction

PROPULSION system designs for proposed commercial supersonic aircraft are likely to include nozzles with internal mixers and external plugs. In addition to the usual jet mixing noise, these nozzles are observed to contain features which could produce noise from other source mechanisms, such as that generated internal to the nozzle by the mixer and by the interaction of turbulence with the shock wave formed near the nozzle exit. The latter situation is described in Ref. [1], where Figure 12 of that paper shows a Background-Oriented Schliern (BOS) image of a shock near the plug crown – at sub-critical conditions – caused by local flow accelerations over the curvature of the plug profile. The formation of a shock was found to be a consistent feature of the plug nozzles tested in Ref. [1] whenever the crown of the plug was positioned near the nozzle exit. Figure 1 shows BOS images from a test at NASA Glenn (Ref. [2]) of a shock that forms, and grows in strength with increasing nozzle pressure ratio, at sub-critical conditions, over a plug with abrupt curvature change. In these images, the flow is from right to left and the plug occupies the white space. It has been suggested that shear-layer interaction with this shock might be responsible for the additional, near-omi-directional, sound component measured in the tests (Ref. [1]).

A similar mechanism appears to occur at the transition between the convergent and final parallel sections of nozzles with internal forced mixers but without a plug (Refs. [3], [4], [5]). Computational Fluid Dynamics analysis of the forced mixer geometry (Ref. [6]) seems to support the notion that additional noise found at higher Mach numbers was due to the interaction of turbulence with a normal shock near the nozzle exit. It was suggested in those papers that a linear inviscid analysis may be useful for the prediction of noise from this mechanism. This paper is concerned with the development and implementation of a method for assessing the significance of the noise generated by the turbulence/shock interaction mechanism in the internally mixed/externally plugged nozzle geometries under consideration for commercial supersonic aircraft.

Linear inviscid approaches to the study of flow modifications and noise generation by a turbulent flow field passing through a shock were originally formulated by Moore [7] and Ribner [8]. In particular, Ribner [9], [10] employed these techniques to study sound generated by this process. The approach has come to be called the Linear Interaction Approximation (LIA) and details of the formulation are presented in the book by Sagaut & Cambon [11]. The basic formulation is also outlined and applied to particular problems in numerous papers (See Refs. [12], [13] [14], [15] and [16], to cite just a few). The linear formulation has also been extended to include weakly non-linear effects (Ref. [17])to extend the range of applicability. The approach uses the linearized Euler equations, along with the Kovaszany [18]

*Senior Engineer, AIAA Senior Member



Fig. 1 BOS images of shocks in an externally plugged nozzle at sub-critical conditions. From [2], used with permission.

decomposition, in conjunction with the Rankine-Hugoniot relations (Ref. [19]), to relate the flow fields upstream and downstream of the shock. In the linear theory, independent plane wave components of the vorticity, entropy and/or acoustic modes of the Kovaszany decomposition can be considered to be incident on the shock, generating a triad of all three modes downstream. Solutions for individual Fourier components can then be summed to obtain results for an turbulent incident flow with specified energy spectrum.

In this paper we review the basic formulation of the method and apply it to generic cases of (separate) isotropic turbulence (vortical) and entropy fields incident on a planar shock wave. With the basic formulation implemented and demonstrated, we discuss applications more particular to the internally mixed/externally plugged nozzles envisioned for commercial supersonic aircraft, which will be the subject of future efforts. The focus of this paper is on the noise (acoustic mode) generated downstream of the shock by the interaction of vorticity and entropy modes, but the formulation can also be used to investigate the modification of the turbulence (vorticity mode), ie. the mixing noise sources, when passing through the shock and, with minor extension, to the noise (acoustic mode) scattered by the shock by an incident acoustic field. The ultimate goal of this work is the development of a tool that can be used to assess the impact on noise of the shock formed near the nozzle exit in commercial supersonic exhaust system designs.

The plan of the paper is as follows. In Section II the basic formulation of LIA is reviewed. The particular cases of incident vorticity and entropy modes are developed in Sections III and IV, respectively. Numerical results are presented Section V, and Section VI discusses the results and future applications envisioned for the theory.

II. Formulation

The main assumptions of LIA are that: (1) the turbulent perturbations are relatively weak and the distorted shock wave remains well defined, (2) the time scale over which the interactions take place is short relative to the time scale of the turbulence evolution, so that the problem may be linearized and viscous effects neglected.

The main analysis is two-dimensional and is extended to three dimensions to obtain results representative of an incident turbulent flow field (See Ref. [11]).

A. Governing equations

The governing equations are the Euler equations,

$$\frac{\partial \rho}{\partial t} + \nabla \cdot (\rho \boldsymbol{u}) = 0, \tag{1}$$

$$\rho(\frac{\partial \boldsymbol{u}}{\partial t} + \boldsymbol{u} \cdot \nabla \boldsymbol{u}) + \nabla p = 0, \tag{2}$$

$$\frac{\partial s}{\partial t} + \boldsymbol{u} \cdot \nabla s = 0, \tag{3}$$

where ρ is the density $\boldsymbol{u}$ the velocity, p the pressure and s the entropy, with the ideal gas law

$$p = \rho R T, \tag{4}$$

where R is the gas constant and T is the temperature. The entropy is given relative to a reference state (denoted with subscript r) by

$$s - s_r = c_v \log[\frac{p}{p_r}(\frac{\rho_r}{\rho})^\gamma], \tag{5}$$

with $\gamma = \frac{c_p}{c_v}$, c_p and c_v are the specific heats at constant pressure and volume, respectively.

These are linearized about a uniform base flow $\{\bar{\rho}, \bar{\boldsymbol{u}}, \bar{p}, \bar{s}\}$

$$\boldsymbol{u}(\boldsymbol{x}, t) = \bar{\boldsymbol{u}} + \epsilon \boldsymbol{u}'(\boldsymbol{x}, t) + \cdots, \tag{6}$$

$$\rho(\boldsymbol{x}, t) = \bar{\rho} + \epsilon \rho'(\boldsymbol{x}, t) + \cdots, \tag{7}$$

$$p(\boldsymbol{x}, t) = \bar{p} + \epsilon p'(\boldsymbol{x}, t) + \cdots, \tag{8}$$

$$s(\boldsymbol{x}, t) = \bar{s} + \epsilon s'(\boldsymbol{x}, t) + \cdots, \tag{9}$$

with ϵ being a small parameter, $\boldsymbol{u} = U\hat{\boldsymbol{i}}$, $\boldsymbol{x} = (x\hat{\boldsymbol{i}}, y\hat{\boldsymbol{j}}, z\hat{\boldsymbol{k}})$ and t is time, obtain

$$\frac{\bar{D}\rho'}{Dt} + \bar{\rho}\nabla \cdot \boldsymbol{u}' = 0, \tag{10}$$

$$\frac{\bar{D}\boldsymbol{u}'}{Dt} + \frac{1}{\bar{\rho}}\nabla p' = 0, \tag{11}$$

$$\frac{\bar{D}s'}{Dt} = 0, \tag{12}$$

where

$$\frac{\bar{D}}{Dt} = \frac{\partial}{\partial t} + \bar{\boldsymbol{u}} \cdot \nabla. \tag{13}$$

The linearized equation of state becomes

$$p' = \rho' R\bar{T} + \bar{\rho} R T', \tag{14}$$

and the fluctuating entropy is defined by

$$s' = c_v(\frac{p'}{\bar{p}} - \gamma\frac{\rho'}{\bar{\rho}}). \tag{15}$$

Equations (10) - (15) can be used to derive separate equations for the fluctuating vorticity, $\boldsymbol{\Omega}' = \nabla \times \boldsymbol{u}'$, and fluctuating pressure as

$$\frac{\bar{D}\boldsymbol{\Omega}'}{Dt} = 0, \tag{16}$$

and

$$\frac{\bar{D}^2 p'}{Dt^2} - \bar{a}^2 \nabla^2 p' = 0, \tag{17}$$

where $\bar{a}^2 = \frac{\gamma \bar{p}}{\bar{\rho}}$ is the square of the mean speed of sound. Then equations (12), (16) and (17) provide equations for the fluctuating entropy, vorticity and pressure, respectively.

B. Kovaszany decomposition

Kovaszany (Ref. [18]) showed that the linearized unsteady motion about a uniform base flow can be decomposed into independent vorticity, entropy and acoustic modes, defined as

1) Vorticity mode, $\{\boldsymbol{\Omega_v}, p_v, s_v, \boldsymbol{u}_v\}$:

$$\frac{\bar{D}\boldsymbol{\Omega}_v}{Dt} = 0 \tag{18}$$

$$\boldsymbol{\Omega}_v = \nabla \times \boldsymbol{u}_v, \quad p_v = s_v = 0, \quad \nabla \cdot \boldsymbol{u}_v = 0. \tag{19}$$

2) Entropy mode, $\{\boldsymbol{\Omega_e}, p_e, s_e, \boldsymbol{u}_e\}$:

$$\frac{\bar{D}s_e}{Dt} = 0 \tag{20}$$

$$\boldsymbol{\Omega}_e = p_e = \boldsymbol{u}_e = 0, \tag{21}$$

3) Acoustic mode, $\{\boldsymbol{\Omega_p}, p_p, s_p, \boldsymbol{u}_p\}$:

$$\frac{\bar{D}^2 p_p}{Dt^2} - \bar{a}^2 \nabla^2 p_p = 0. \tag{22}$$

$$\boldsymbol{\Omega}_p = \nabla \times \boldsymbol{u}_p = 0, \quad \frac{\bar{D}s_p}{Dt} = 0, \quad \nabla \cdot \boldsymbol{u}_p = -\frac{\bar{D}p_p}{Dt}. \tag{23}$$

The velocity field of the vorticity mode is solenoidal, this mode carries no pressure fluctuations at leading order and its vorticity is purely convected by the mean flow. The velocity field of the entropy mode is dilitational (it is zero in the invisicid case), it also has no pressure fluctuations and its entropy is purely convected by the mean flow. The acoustic mode carries all the pressure fluctuations and is irrotational. In the linear approximation these modes are uncoupled and the decomposition allows for the specification of individual modes incident on a shock. However, after passing through the discontinuity of the shock, any incident mode triggers all three types of modes on the other side. In this work we will be concerned with incident vorticity and entropy modes of plane wave form, being representative of Fourier components of a turbulent flow, and the generation of acoustic modes by their interaction with the shock. Results for different Fourier components will then be combined to obtain results for an incident turbulent flow with a particular spectral distribution to determine statistics of the sound field generated.

C. Jump conditions across the shock

The shock is modeled as a surface discontinuity of zero thickness in the (y, z) plane and the jumps in flow quantities across it are described by the Rankine-Hugoniot conditions

$$[\![\rho u_n]\!] = 0, \tag{24}$$

$$[\![\rho u_n^2 + p]\!] = 0, \tag{25}$$

$$[\![\boldsymbol{u}_t]\!] = 0, \tag{26}$$

$$[\![c_p T + \frac{u^2}{2}]\!] = 0, \tag{27}$$

where $[\![q]\!]$ refers to the jump in any quantity, q, across the shock, u_n is the instantaneous velocity component normal to the shock surface, $\boldsymbol{u}_t$ is the instantaneous velocity vector transverse to the shock surface and $u = |\boldsymbol{u}|$.

The linearization of equations (6) - (9) is used to obtain jump conditions on the mean and leading-order fluctuating quantities. We consider the case where the mean flow upstream and downstream of the shock is parallel and entirely in the x direction, denoting it by U_1 and U_2, respectively.

The mean jump conditions are

$$C = \frac{\bar{\rho}_2}{\bar{\rho}_1} = \frac{U_1}{U_2} = \frac{(\gamma+1)M_1^2}{2+(\gamma-1)M_1^2}, \tag{28}$$

$$\frac{\bar{p}_2}{\bar{p}_1} = 1 + \frac{2\gamma(M_1^2-1)}{\gamma+1}, \tag{29}$$

$$\frac{\bar{T}_2}{\bar{T}_1} = \frac{[1+\frac{\gamma-1}{2}M_1^2][\frac{2\gamma}{\gamma-1}M_1^2-1]}{\frac{(\gamma+1)^2M_1^2}{2(\gamma-1)}}, \tag{30}$$

$$M_2 = \frac{U_2}{\bar{a}_2} = \sqrt{\frac{2+(\gamma-1)M_1^2}{2\gamma M_1^2-(\gamma-1)}}, \tag{31}$$

where $M_1 = U_1/\bar{a}_1$ is the Mach number and flow quantities upstream and downstream of the shock are denote by subscript 1 and 2, respectively.

At leading order, the jump conditions on the fluctuating flow are

$$[\![\bar{\rho}(u'-u_s') + \rho'(U-\bar{u}_s)]\!] \equiv [\![j']\!] = 0, \tag{32}$$

$$\bar{j}[\![u']\!] + j'[\![U]\!] + [\![p']\!] = 0, \tag{33}$$

$$[\![U\alpha' + v']\!] = 0, \tag{34}$$

$$[\![c_p T' + (U-\bar{u}_s)(u'-u_s')]\!] = 0, \tag{35}$$

where u' and v' are the fluctuating velocity components in the x and y directions, respectively, α' is the angle between the undisturbed shock front and local tangent to its disturbed position, $\bar{u}_s$ is the mean motion of the shock, u_s' its fluctuating motion, and

$$\bar{j} = \bar{\rho}(U-\bar{u}_s), \tag{36}$$

$$j' = \rho'(U-\bar{u}_s) + \bar{\rho}(u'-u_s'). \tag{37}$$

These conditions are used to determine the mean and fluctuating flow fields downstream of the shock in terms of a specified incident flow upstream.

III. Vorticity Mode Incident on a Stationary Planar Shock

A. Incident mode

In this section we consider the case where a vorticity mode is incident on a stationary planar shock. The incident vorticity mode is described by the Fourier components of its velocity as

$$\begin{Bmatrix} \frac{u_1'}{U_1} \\ \frac{v_1'}{U_1} \\ \frac{\rho_1'}{\bar{\rho}_1} \\ \frac{p_1'}{\bar{p}_1} \\ \frac{T_1'}{\bar{T}_1} \\ \frac{s_1'}{c_p} \end{Bmatrix} = A_v(\boldsymbol{k}) \begin{Bmatrix} \sin\alpha \\ -\cos\alpha \\ 0 \\ 0 \\ 0 \\ 0 \end{Bmatrix} e^{(i(k[x\cos\alpha + y\sin\alpha] - \omega t)} \tag{38}$$

where $A_v(\boldsymbol{k})$ is the amplitude of the incident vorticity mode, α is the angle between the wavenumber vector, $\boldsymbol{k}$, and the x axis and the dispersion relation for this mode requires

$$\omega = U_1 k \cos\alpha. \tag{39}$$

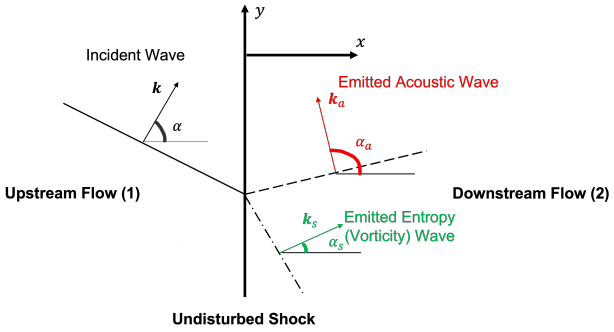


Fig. 2 Two-dimensional LIA schematic

B. Emitted field

The incidence of a vorticity mode on the plane shock generates vorticity, entropy and acoustic modes on the other side. The frequency and transverse wave numbers of the emitted waves are equal to those of the incident one, so that the solution for the emitted field can be expressed as

$$\begin{Bmatrix} \frac{u_2'}{U_2} \\ \frac{v_2'}{U_2} \\ \frac{\rho_2'}{\bar{\rho}_2} \\ \frac{p_2'}{\bar{p}_2} \\ \frac{T_2'}{\bar{T}2} \\ \frac{s_2'}{c_P} \end{Bmatrix} = A_v \begin{Bmatrix} Z_{vv}\sin\alpha_s \\ -Z_{vv}\cos\alpha_s \\ -Z_{vs} \\ 0 \\ Z_{vs} \\ Z_{vs} \end{Bmatrix} e^{(i(k_s[x\cos\alpha_s + y\sin\alpha_s] - \omega t)} + A_v Z_{va} \begin{Bmatrix} \frac{\cos\alpha_a + i\eta}{M_2\zeta} \\ \frac{\sin\alpha_a}{M_2\zeta} \\ 1 \\ 1 \\ (\gamma-1) \\ 0 \end{Bmatrix} e^{-k_a\eta x} e^{(i(k_a[x\cos\alpha_a + y\sin\alpha_a] - \omega t)} \tag{40}$$

where Z_{vi}, with $i = v, s, a$, are the transfer coefficients for the resulting emitted vorticity, entropy and acoustic modes, respectively, $\boldsymbol{k}_s$ is the wavenumber vector of the emitted entropy and vorticity waves (which have the same dispersion relation), α_s is the angle between $\boldsymbol{k}_s$ and the x axis, with $\boldsymbol{k}_a$ and α_a those of the acoustic wave.

The dispersion relation provides the emission angles and wavenumbers of the vorticity and entropy modes as

$$\cot\alpha_s = C\cot\alpha, \tag{41}$$

and

$$\frac{k_s}{k} = \frac{\sin\alpha}{\sin\alpha_s}. \tag{42}$$

For the acoustic wave, there is a propagative and damped regime separated by a critical incidence angle given by

$$\cot\alpha_c = \frac{\sqrt{1-M_2^2}}{CM_2}. \tag{43}$$

The dispersion relation for this wave gives

$$\begin{aligned} C\cot\alpha &= \cot\alpha_a + \frac{1}{M_2\sin\alpha_a}, \text{propagative} \\ \frac{\cot\alpha_a}{\cot\alpha_a^c} &= \frac{\cot\alpha}{\cot\alpha_c}, \text{damped} \end{aligned}, \tag{44}$$

with the damping factor as

$$\eta = \begin{cases} 0 & \text{, propagative} \\ \frac{|\cot\alpha_a^c \cot\alpha_a|}{M_2}\sqrt{1-(\frac{\cot\alpha}{\cot\alpha_c})^2} & \text{, damped} \end{cases}, \tag{45}$$

and

$$\frac{k_a}{k} = \frac{\sin\alpha}{\sin\alpha_a}. \tag{46}$$

The shock displacement can be written as

$$\xi(y,t) = Z_{vx} e^{i(k\sin\alpha y - \omega t)}. \tag{47}$$

Using (38) and (40) in the linearized jump conditions (32) - (35), along with (47), a linear system of equations for the transfer coefficients of the emitted field can be obtained

$$\begin{Bmatrix} \sin\alpha_s & -1 & \frac{1}{\gamma}+\frac{\cos\alpha_a+i\eta}{\gamma M_2\zeta} & i(C-1)\cos\alpha \\ 2\sin\alpha_s & -1 & \frac{1+M_2^2}{\gamma M_2^2}+2\frac{\cos\alpha_a+i\eta}{\gamma M_2\zeta} & 0 \\ -\cos\alpha_s & 0 & \frac{\sin\alpha_a}{\gamma M_2\zeta} & i(C-1)\sin\alpha \\ \sin\alpha_s & \frac{1}{(\gamma-1)M_2^2} & \frac{1}{\gamma M_2^2}+\frac{\cos\alpha_a+i\eta}{\gamma M_2\zeta} & iC(C-1)\cos\alpha \end{Bmatrix} \begin{Bmatrix} Z_{vv} \\ Z_{vs} \\ Z_{va} \\ Z_{vx} \end{Bmatrix} = \begin{Bmatrix} \sin\alpha \\ 2C\sin\alpha \\ -C\cos\alpha \\ C^2\sin\alpha \end{Bmatrix}. \tag{48}$$

The system (48) can be solved for the transmission coefficients $Z_{vv}, Z_{vs}, Z_{va}, Z_{vx}$ to obtain the amplitudes of the fluctuating flow variables downstream of the shock.

C. Extension to three dimensions

The two-dimensional analysis outlined above can be extended to three dimensions by noting that velocity components transverse to the shock surface are unmodified through the shock and applying the two-dimensional analysis in the axial-radial plane in cylindrical coordinates. Details are given in Refs. [11] and [14]. Then the single-wave component results can be combined to obtain the flow field downstream of the shock due to a incident turbulent flow field with specified energy spectrum.

D. Evaluation of the downstream acoustic field for an incident turbulent flow

By combining solutions for individual Fourier components of vorticity modes, we can consider the incidence of an incompressible incident turbulence field. In this paper we will consider an isotropic incident turbulence field whose energy spectrum is given by (Ref. [20])

$$E_{ij}(\boldsymbol{k}) = \frac{E(k)}{4\pi k^2}(\delta_{ij} - \frac{k_i k_j}{k^2}) \tag{49}$$

where $E(k)$ is the three-dimensional energy spectrum. Then the amplitudes of the incident single-wave components of the vorticity mode are given by (Ref. [11])

$$|A_v|^2 = \frac{E(k)}{4\pi k^2}. \tag{50}$$

The variance of the emitted pressure for a single Fourier component is obtained from (40) as

$$\frac{\overline{p_2'^2}(x;k,\alpha)}{\bar{p_2}^2} = |A_v|^2|Z_a|^2 e^{-2k_a\eta x} = \frac{E(k)}{4\pi k^2}|Z_{va}|^2 e^{-2k_2\eta x}. \tag{51}$$

Then integrating over all wavenumbers (magnitude and direction) gives the emitted pressure variance due to an incident isotropic turbulence field as

$$\frac{\overline{p_2'^2}(x)}{\bar{p_2}^2} = \frac{1}{2}\int_0^\infty \int_0^{\pi/2} E(k)|Z_{va}|^2 e^{-2k_a\eta x}\sin\alpha d\alpha dk, \tag{52}$$

with its three-dimensional spectrum being

$$E_{pp}(k) = \frac{1}{2}E(k)\int_0^{\frac{\pi}{2}} |Z_{va}|^2 e^{-2k_a\eta x}\sin\alpha d\alpha. \tag{53}$$

Potential choices for the three-dimensional spectrum, $E(k)$, of the incident turbulent flow will be discussed in section V where numerical results are presented.

IV. Entropy Mode Incident on a Stationary Planar Shock

The exhaust flows from the internally mixed/externally plugged nozzles being designed for commercial supersonic applications are heated and noise can also be generated by high-temperature 'spots' passing through the shock formed near the nozzle exit at the plug crown. To represent this situation, we consider the case of an incident entropy mode on a planar shock wave.

The analysis for the transmitted vorticity, entropy, acoustic and displacement waves due to single-wave components of an incident entropy mode carries through in a manner very similar to that for the single vorticity waves in section III.

The incident field is given as

$$\begin{Bmatrix} \frac{u_1'}{U_1} \\ \frac{v_1'}{U_1} \\ \frac{\rho_1'}{\bar{\rho}_1} \\ \frac{p_1'}{\bar{p}_1} \\ \frac{T_1'}{\bar{T}_1} \\ \frac{s_1'}{c_p} \end{Bmatrix} = A_s(\boldsymbol{k}) \begin{Bmatrix} 0 \\ 0 \\ -1 \\ 0 \\ 1 \\ 1 \end{Bmatrix} e^{(i(k[x\cos\alpha + y\sin\alpha] - \omega t)}, \tag{54}$$

where $A_s(\boldsymbol{k})$ is the amplitude of the incident entropy mode.

The emitted field can be expressed as

$$\begin{Bmatrix} \frac{u_2'}{U_2} \\ \frac{v_2'}{U_2} \\ \frac{\rho_2'}{\bar{\rho}_2} \\ \frac{p_2'}{\bar{p}_2} \\ \frac{T_2'}{\bar{T}2} \\ \frac{s_2'}{c_p} \end{Bmatrix} = A_s \begin{Bmatrix} Z_{sv}\sin\alpha_s \\ -Z_{sv}\cos\alpha_s \\ -Z_{ss} \\ 0 \\ Z_{ss} \\ Z_{ss} \end{Bmatrix} e^{(i(k_s[x\cos\alpha_s + y\sin\alpha_s] - \omega t)} + A_s Z_{sa} \begin{Bmatrix} \frac{\cos\alpha_a + i\eta}{M_2\zeta} \\ \frac{\sin\alpha_a}{M_2\zeta} \\ 1 \\ 1 \\ (\gamma - 1) \\ 0 \end{Bmatrix} e^{-k_a\eta x} e^{(i(k_a[x\cos\alpha_a + y\sin\alpha_a] - \omega t)}, \tag{55}$$

where Z_{si}, with $i = v, s, a$, are the transfer coefficients for the emitted vorticity, entropy and acoustic modes, respectively, due to the incidnet entropy mode, and the transfer coefficients can be obtained by solution of

$$\begin{Bmatrix} \sin\alpha_s & -1 & \frac{1}{\gamma} + \frac{\cos\alpha_a + i\eta}{\gamma M_2\zeta} & i(C-1)\cos\alpha \\ 2\sin\alpha_s & -1 & \frac{1+M_2^2}{\gamma M_2^2} + 2\frac{\cos\alpha_a + i\eta}{\gamma M_2\zeta} & 0 \\ -\cos\alpha_s & 0 & \frac{\sin\alpha_a}{\gamma M_2\zeta} & i(C-1)\sin\alpha \\ \sin\alpha_s & \frac{1}{(\gamma-1)M_2^2} & \frac{1}{\gamma M_2^2} + \frac{\cos\alpha_a + i\eta}{\gamma M_2\zeta} & iC(C-1)\cos\alpha \end{Bmatrix} \begin{Bmatrix} Z_{sv} \\ Z_{ss} \\ Z_{sa} \\ Z_{sx} \end{Bmatrix} = \begin{Bmatrix} -1 \\ -C \\ 0 \\ \frac{C^2}{(\gamma-1)M_1^2} \end{Bmatrix}. \tag{56}$$

Note that the coefficient matrix in (56) is the same as in (48) and that only the right-hand sides are different due to the different incident modes.

Solutions for individual Fourier components of incident entropy modes can similarly be combined to consider an incident entropy field. In order to obtain an amplitude scaling and a functional form for the spectrum of an incident entropy field we employ Morkovin's hypothesis (Refs. [14], [21])

$$\frac{\rho_1'}{\bar{\rho}_1} = \frac{T_1'}{\bar{T}_1} = -\frac{s_1'}{c_p} = (\gamma-1)M_1^2\frac{u_1'}{U_1}, \tag{57}$$

and consider an isotropic incident field, so that

$$|A_s(\boldsymbol{k})|^2 = (\gamma-1)^2 M_1^4 \sin^2\alpha \frac{E(k)}{4\pi k^2}. \tag{58}$$

Then the variance of the emitted pressure for a single Fourier component of an incident entropy mode is given from (55) as

$$\frac{\overline{p_2'^2}(x;k,\alpha)}{\bar{p_2}^2} = (\gamma-1)^2 M_1^4 \sin^2\alpha \frac{E(k)}{4\pi k^2}|Z_{sa}|^2 e^{-2k_2\eta x}, \tag{59}$$

the emitted pressure field due to an incident isotropic entropy field is obtained as

$$\frac{\overline{p_2'^2}(x)}{\bar{p_2}^2} = (\gamma-1)^2 M_1^4 \frac{1}{2}\int_0^\infty \int_0^{\pi/2} E(k)|Z_{sa}|^2 e^{-2k_a\eta x}\sin^3\alpha d\alpha dk, \tag{60}$$

and its three-dimensional spectrum is

$$E_{pp}(k) = (\gamma-1)^2 M_1^4 \frac{E(k)}{2}\int_0^{\frac{\pi}{2}} |Z_{sa}|^2 e^{-2k_a\eta x}\sin^3\alpha d\alpha. \tag{61}$$

In the next section we present numerical results for the acoustic fields emitted by incident vorticity and entropy modes.

V. Results

Results are presented for (separate) incident vorticity and entropy modes based on the formulations in Sections III and IV. Note that the incidence of either a single-wave component of vorticity or entropy mode generates emitted vorticity, entropy and acoustic waves at the same emission angles (these waves have the same dispersion relation) and that only the emitted amplitudes are changed upon imposing different mode types upstream. We therefore begin by presenting results for the emission angles of the acoustic, vorticity, and entropy waves, and the damping factor for the emitted acoustic waves, as functions of the angle of incident vorticity or entropy waves and the shock strength. Then results are shown for the acoustic field triggered by an incident vorticity mode, first for single-wave components and then for an incident isotropic turbulence field. Finally acoustic results for incident entropy modes are presented.

A. Emission angles and acoustic-mode damping factors

One measure of the shock strength is the ratio of the mean pressures downstream and upstream of the discontinuity (Ref. [12]). This can be expressed in terms of the upstream Mach number from (29) as

$$\chi = 1 + \frac{2\gamma}{\gamma+1}(M_1^2 - 1). \tag{62}$$

Figure 3 shows the relation between this definition of the shock strength and the upstream Mach number, assuming a value for the ratio of specific heats of 1.4.

Figure 4 shows the critical angle of incidence of a single-wave vorticity or entropy mode, beyond which emitted acoustic modes are damped in the mean-streamwise direction, vs. shock strength as defined in (62). This critical angle ranges between 62° and 67° over this range of shock strengths and plays an important role in delineating the propagating and damped regions of emitted acoustic waves.

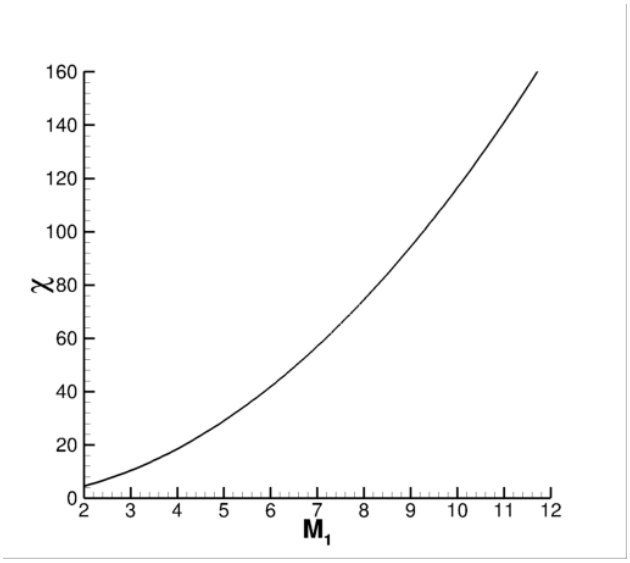


Fig. 3 Shock strength, $\chi = \frac{\bar{p}_2}{\bar{p}_1}$, vs. upstream Mach number, M_1.

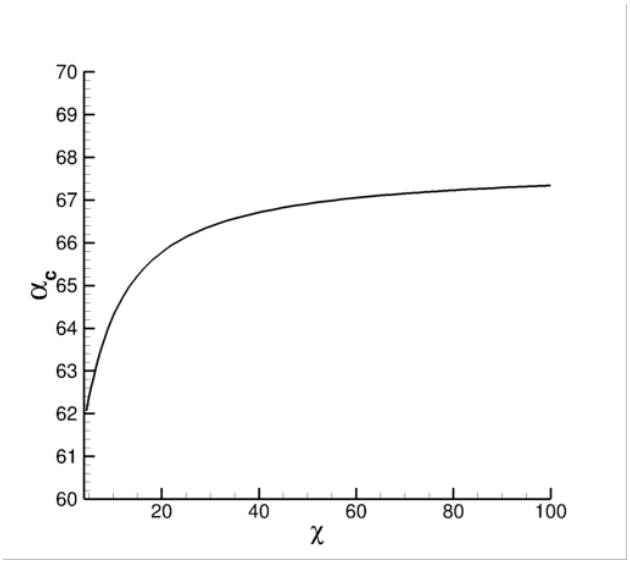


Fig. 4 Critical angle of incidence for propagative acoustic waves vs. shock strength.

Figure 5 shows results computed from (41) and (44) for the emission angles of the acoustic, α_a, and vorticity and entropy, α_s, mode waves (recall that these latter two modes have the same emission angle) and the damping factor, η, of the emitted acoustic wave, vs. the incident angle at upstream Mach numbers ranging from 2.0 to 8.0. The emission angles of the acoustic mode undergo a sharp change at the critical angles of incidence, α_c, beyond which the damping factor becomes non-zero. The damping factor rises quickly beyond the critical angle, so that the acoustic waves emitted by incident vorticity or entropy waves at these angles do not appear in the pressure field far downstream from the shock. The emission angles do not depend strongly on the shock strength over this range, and appear to become independent of it beyond about $M_1 = 4$, as seen in the results in Figure 6 which shows plots of these angles vs. M_1 at a few incident angles.

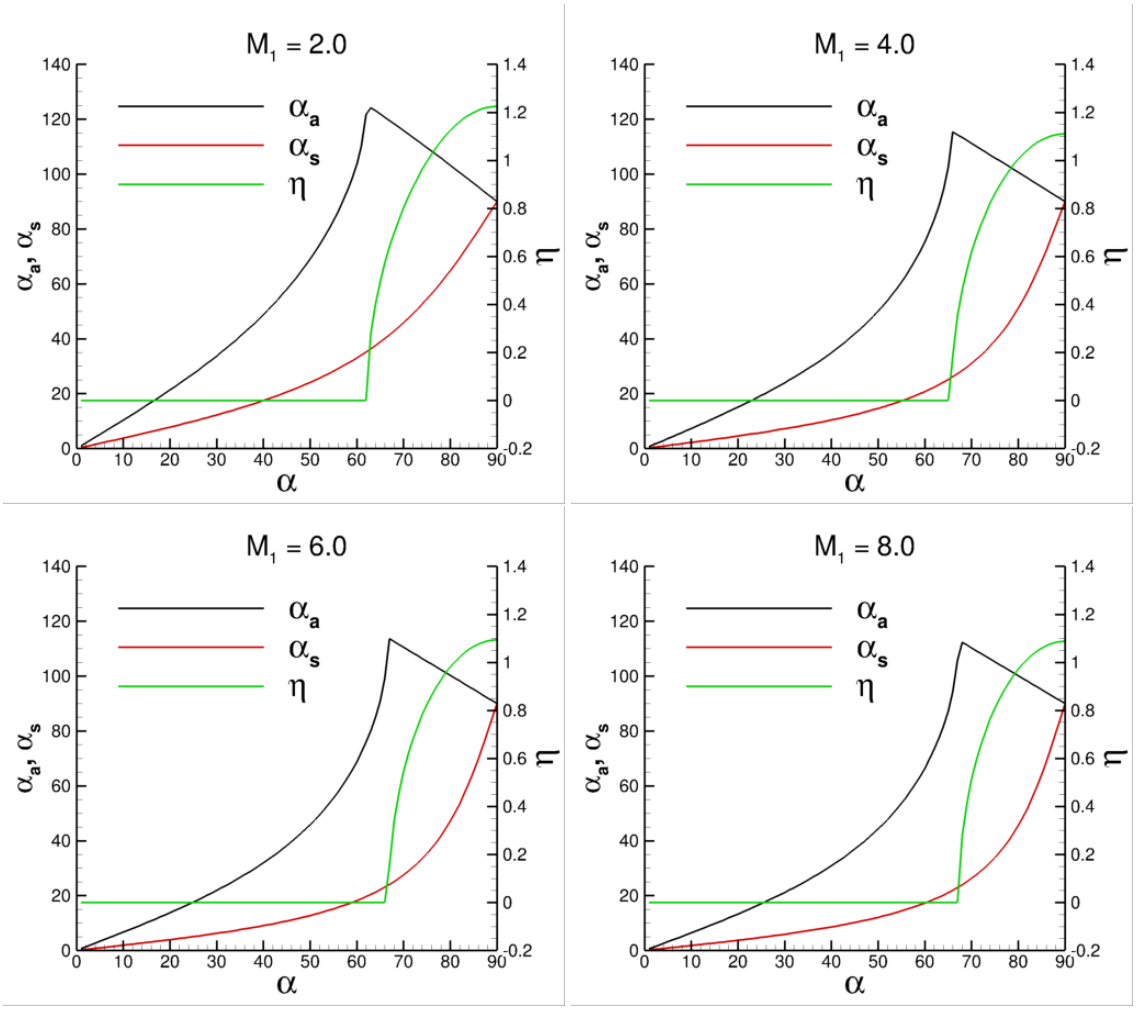


Fig. 5 Angles of emission for the acoustic (α_a) and vorticity and entropy (α_s) mode waves and damping factor (η) of emitted acoustic waves vs. incident angle; $M_1 = 2, 0, 4.0, 6.0, 8.0$**.**

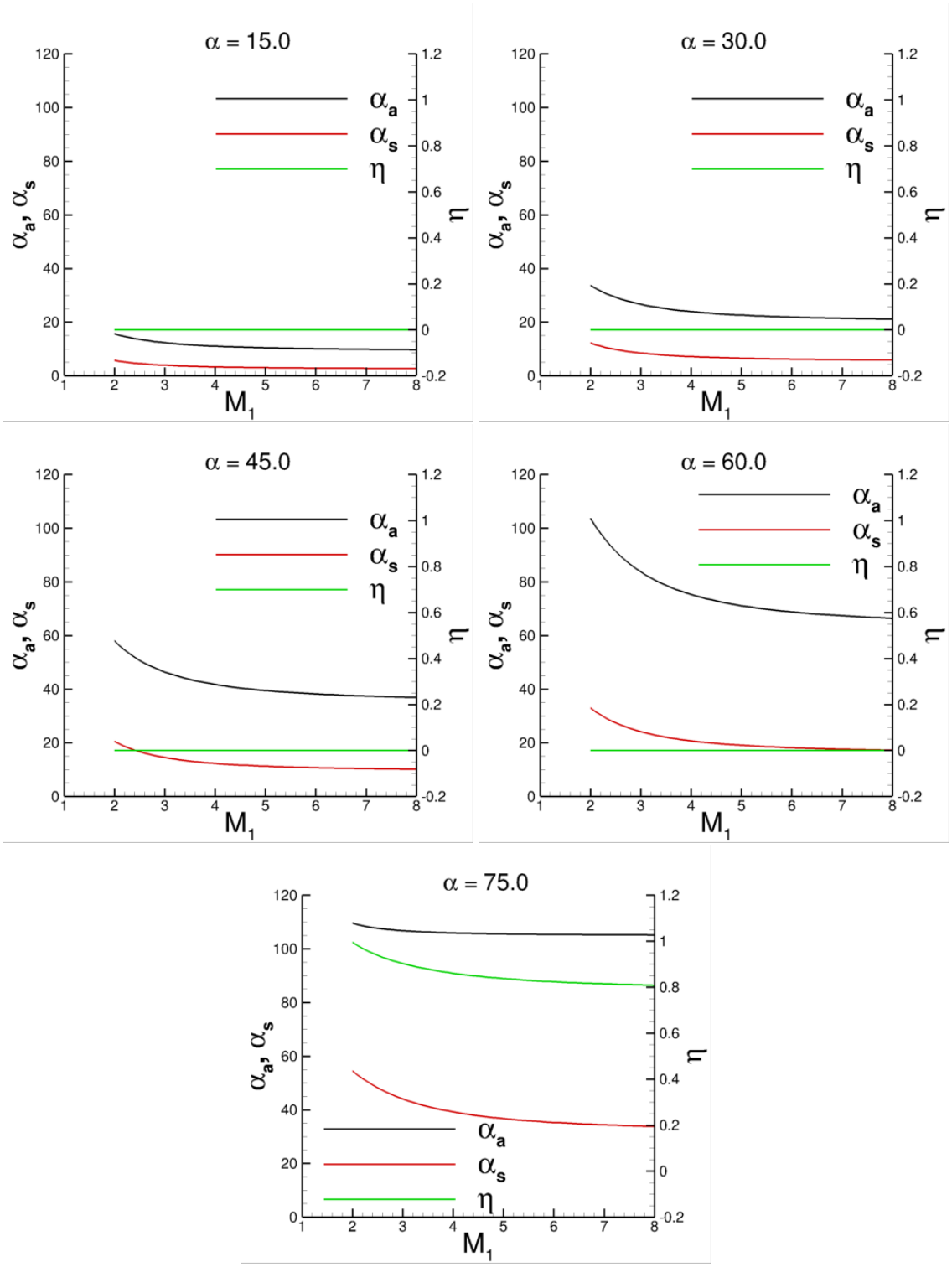


Fig. 6 Angles of emission for the acoustic (α_a) and vorticity and entropy (α_s) mode waves and damping factor (η) of emitted acoustic waves vs. incident Mach number ; $\alpha = 15°, 30°, 45°, 60°,$ **and** $75°$**.**

B. Incident vorticity mode

In this subsection we present results for an incident vorticity mode, representing elements of a turbulent flow. We begin by presenting results for single-wave components and then combine these to obtain results for an incident turbulent flow with a specified spectral form.

1. Transfer coefficients and emitted acoustic field for single-wave components of an incident vorticity mode

In this subsection, results are presented for the transfer coefficients of the emitted waves and the mean-square pressure due to single-wave components of the vorticity mode.

Figures 7 - 10 show the real and imaginary parts and the magnitudes of the transfer coefficients of the emitted vorticity, entropy, acoustic and displacement mode waves, $Z_{vv}, Z_{vs}, Z_{va}, Z_{vx}$, respectively, vs. the vorticity-mode-wave incident angle at upstream Mach numbers ranging from 2.0 to 8.0. Note that for incident angles $\alpha < \alpha_c$, the emitted vorticity, entropy and acoustic waves are in phase with the incident vorticity waves, whereas the displacement mode is out of phase. The vorticity mode wave undergoes a large amplification over this range of incident angles at these upstream Mach numbers, suggesting an increase in the turbulence levels downstream of the shock. In contrast the entropy mode wave triggered downstream of the shock is of much lower amplitude. Our primary interest here is in the emitted acoustic mode waves, which also have modest amplitudes over emission angles less than the critical value, but experience a large increase beyond the critical angle. Although these latter waves are damped in the streamwise direction, the results suggest that the pressure fluctuations immediately downstream of the shock may be relatively large. It should be noted, however, that the liner theory is subject to the most error in this region.

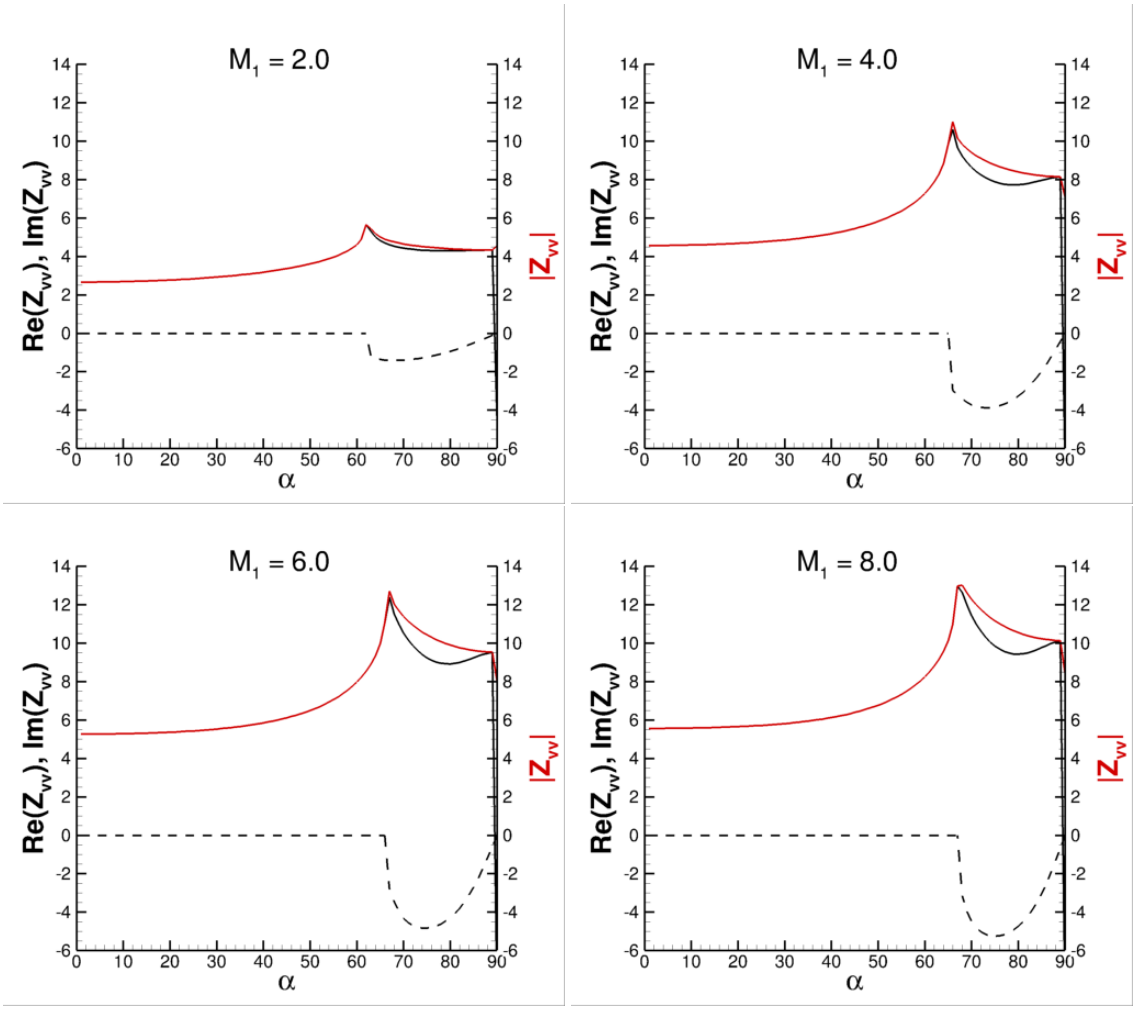


Fig. 7 Transfer coefficient for emitted Vorticity mode wave vs. incident Vorticity mode angle; $M_1 = 2.0, 4.0, 6.0, 8.0$**. Solid black lines - Real, Dashed black lines - Imaginary and Solid red lines - Magnitude.**

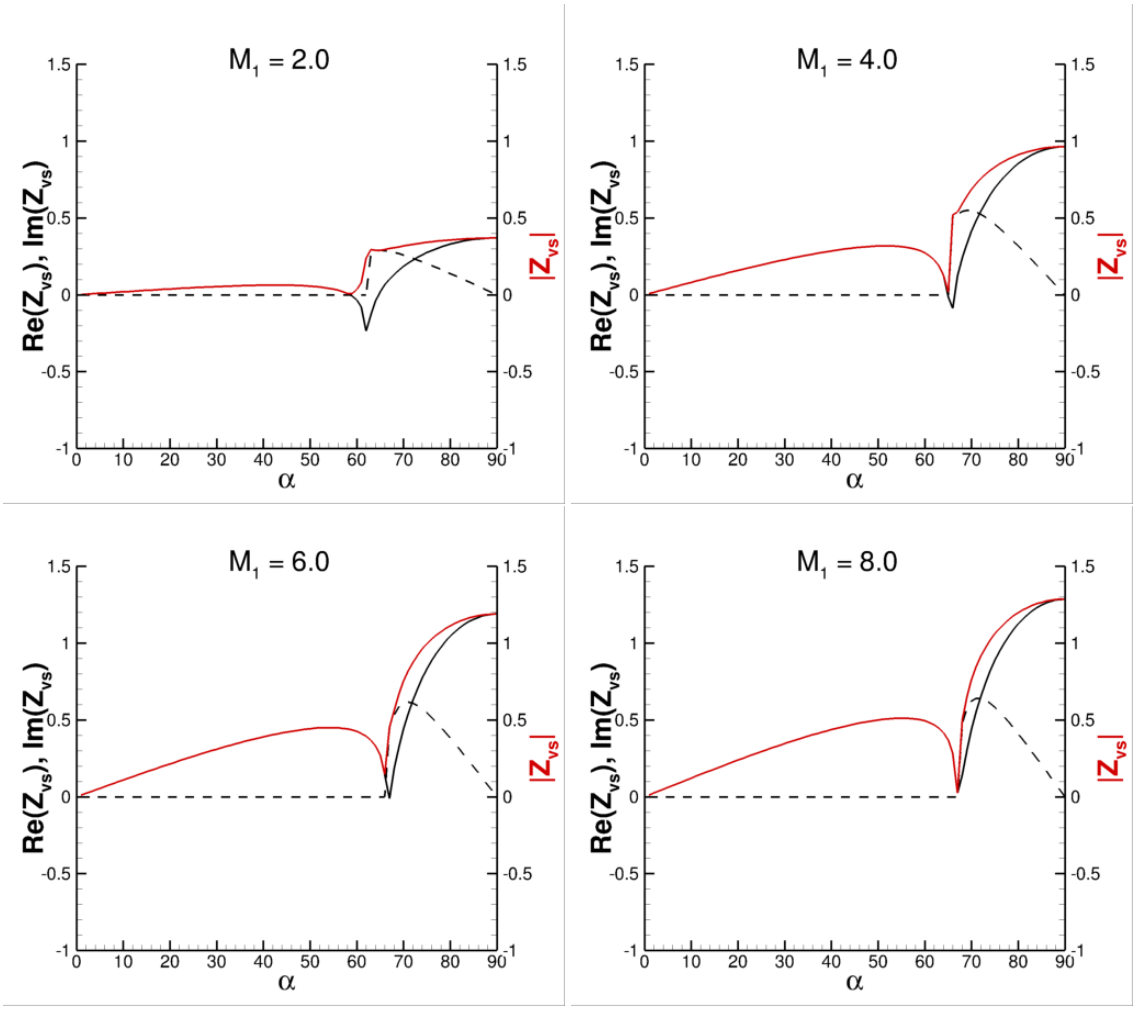


Fig. 8 Transfer coefficient for emitted Entropy mode wave vs. incident Vorticity mode angle; $M_1 = 2.0, 4.0, 6.0, 8.0$**. Solid black lines - Real, Dashed black lines - Imaginary and Solid red lines - Magnitude.**

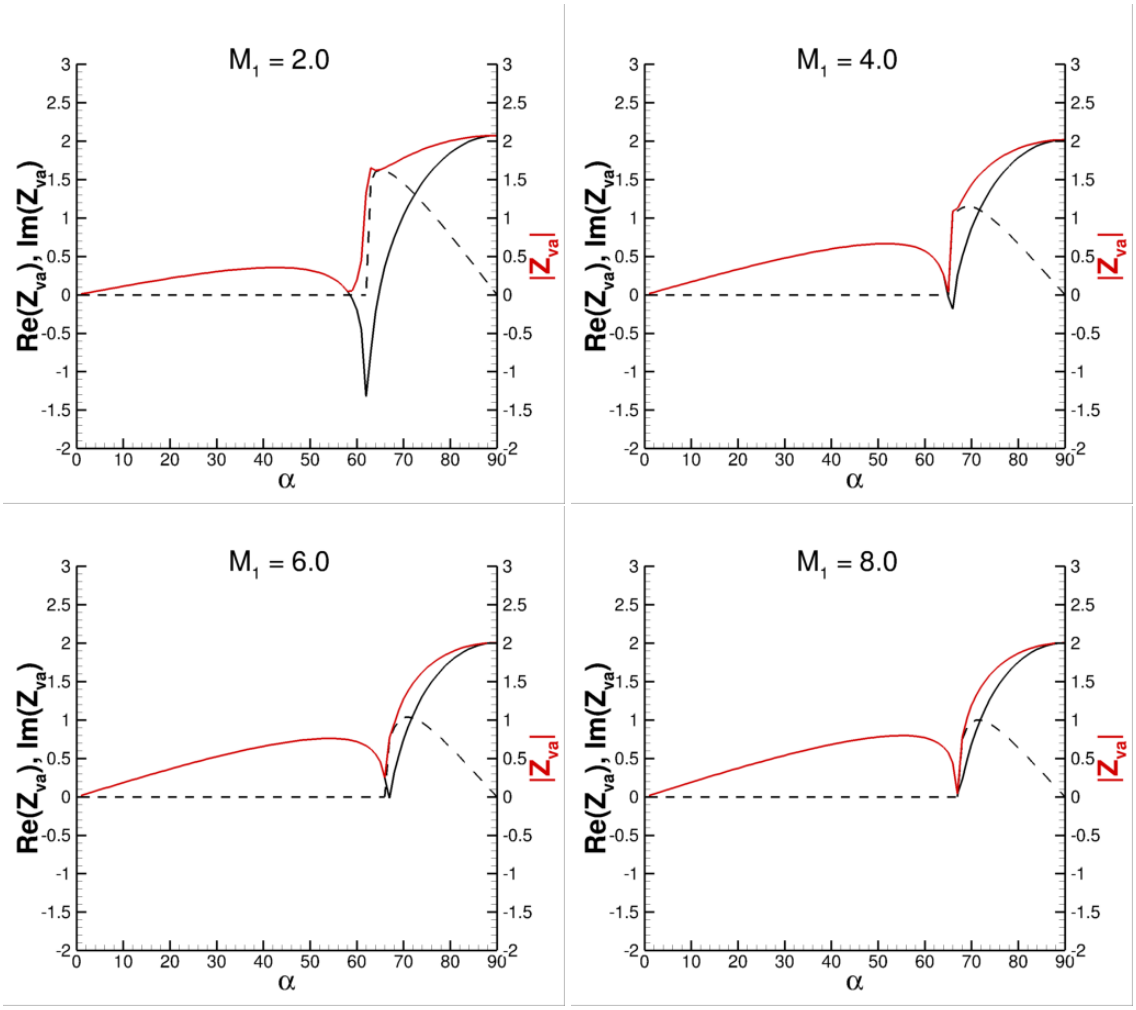


Fig. 9 Transfer coefficient for emitted Acoustic mode wave vs. incident Vorticity mode; $M_1 = 2.0, 4.0, 6.0, 8.0$. Solid black lines - Real, Dashed black lines - Imaginary and Solid red lines - Magnitude.

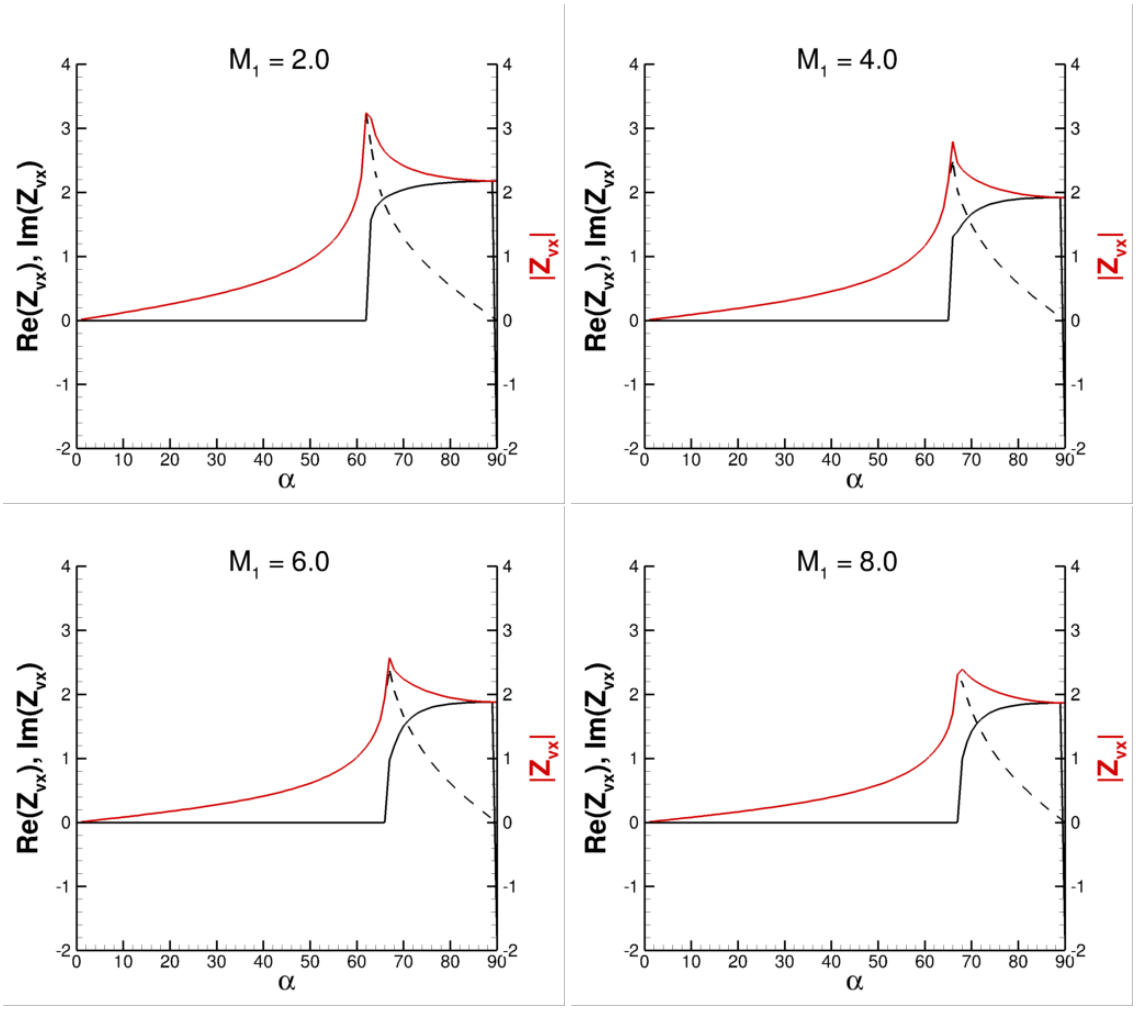


Fig. 10 Transfer coefficient for emitted Displacement wave vs. incident Vorticity mode; $M_1 = 2.0, 4.0, 6.0, 8.0$**.Solid black lines - Real, Dashed black lines - Imaginary and Solid red lines - Magnitude.**

Figure 11 shows the real and imaginary parts of the transfer coefficients vs. the upstream Mach number for a number of angles of incidence of the vorticity mode wave. Note that the transfer coefficients of the vorticity, entropy and acoustic mode waves are purely real, and those of the displacement mode wave purely imaginary, for incident angles below the critical value and in this figure only the curves for $\alpha = 75°$ are in the damped regime of the acoustic waves.

The amplification of the vorticity mode wave initially increases modestly with increasing upstream Mach number before leveling off, with the largest increase (a factor of about two over this Mach number range) being for the incident angle, $\alpha = 75°$. As was seen in Figure 9, the emitted acoustic mode wave has relatively large amplitude for incident angles in the damped regime and drops off very slightly with increasing M_1 before leveling off.

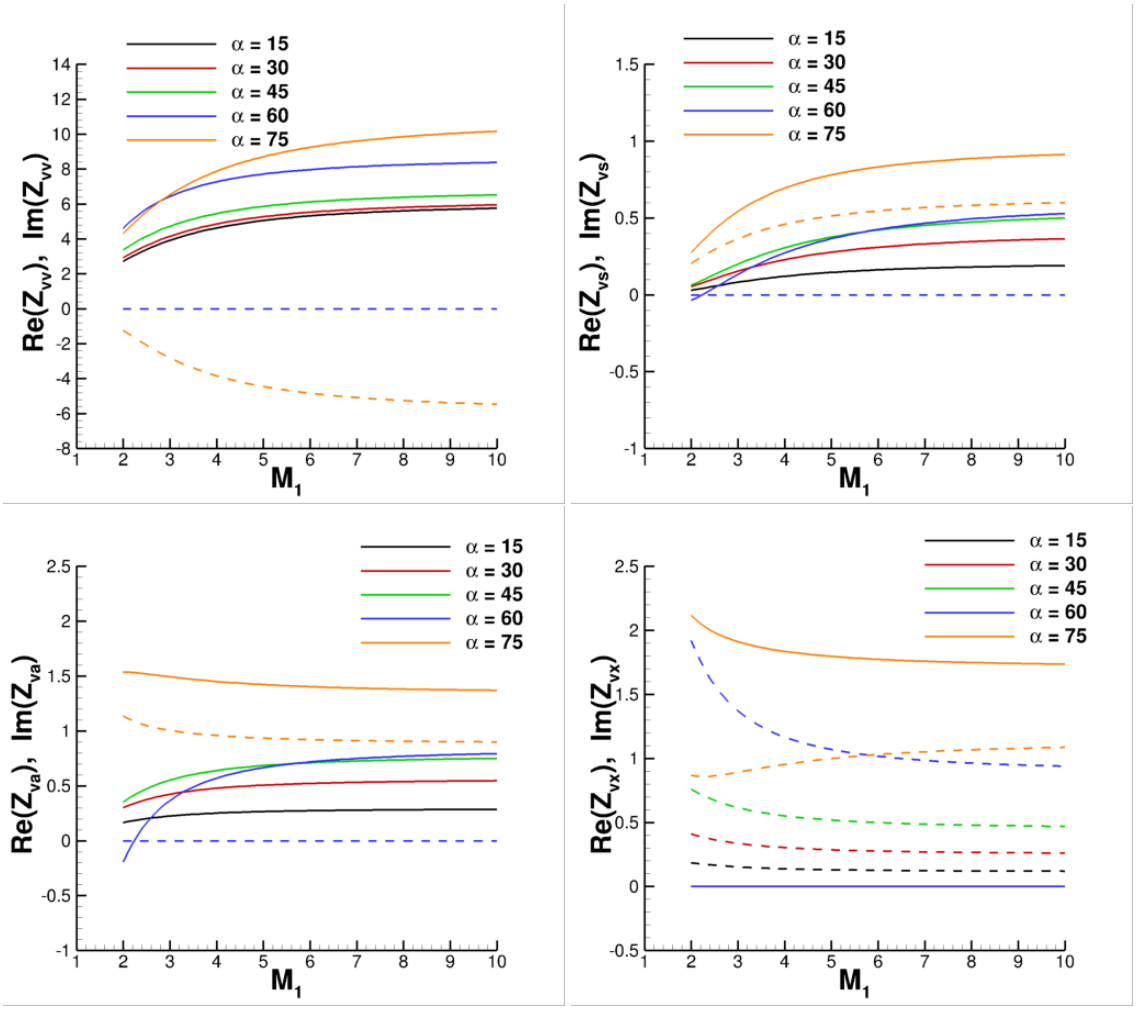


Fig. 11 Transfer coefficients for emitted Vorticity, Entropy, Acoustic and Displacement waves vs. M_1; Incident Vorticity wave angles $\alpha = 15, 30, 45, 60, 75$. Solid lines - Real, Dashed lines - Imaginary.

Figure 12 shows results for the root-mean-square (rms) amplitude of the downstream pressure, normalized by the downstream mean pressure, due to an incident single-wave vorticity mode component vs. incidence angle for different streamwise locations downstream of the shock, normalized by the wavenumber magnitude, for upstream Mach numbers ranging from to 2.0 to 8.0.

As suggested by the results for the transfer coefficients, the emitted pressure rms undergoes a large increase as the critical angle of incidence is approached at locations just downstream of the shock. The large increase in the damping factor beyond the critical incidence angle (Fig. 5) however, results in these wave components not contributing to the far-field pressure fluctuations. The variation of the pressure rms with incident angle become independent of the upstream Mach number (or strength strength) beyond about $M_1 = 4$.

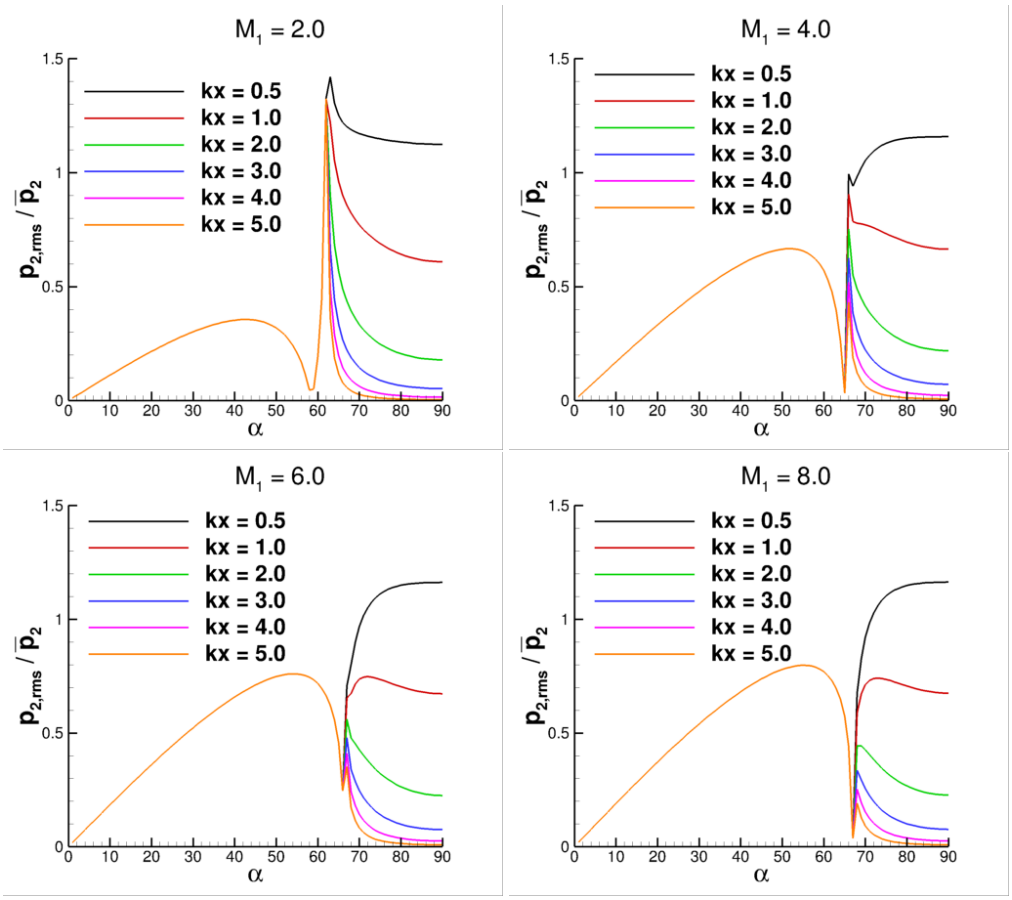


Fig. 12 Normalized root mean square amplitude of the downstream pressure, normalized by the downstream mean pressure, for individual incident vorticity-mode waves vs. α for various distances downstream of the shock, normalized by wavenumber magnitude, at different upstream Mach numbers.

The results for incident single-wave vorticity modes give some information on the form of the flow downstream of the shock, but their real value, in the context of a linear theory, is that they can be combined to calculate the downstream fields triggered by the incidence of a turbulence flow on the shock. In the next subsection we present results for the emitted acoustic field due to an incident isotropic turbulent flow.

2. Emitted pressure field due to an incident isotropic turbulence field

In this subsection we present results obtained by combining the single-wave vorticity mode results of sub-section V.B.1 to obtain the downstream acoustic field for an incident isotropic turbulence field using the formulation in subsection III.D. In the first set of results, we consider a three-dimensional energy spectrum given by (Ref. [20])

$$E(k) = \frac{(k/k_0)^4}{\left[1 + (k/k_0)^2\right]^{17/6}}, \tag{63}$$

where k_0 is the peak in the spectrum.

Figure 13 shows results for the downstream pressure variance, normalized by the downstream mean pressure, vs. streamwise distance downstream of the shock, normalized by the peak wavenumber of the incident spectrum, at various upstream Mach numbers. As suggested by the single-wave results, the emitted pressure variance due to an incident isotropic turbulence field has its highest levels at locations immediately downstream of the shock. This peak level quickly drops with increasing distance from the shock, as the damped emitted waves decay, and the pressure variances become independent of xk_0 with levels that increase with increasing Mach number until about $M_1 = 6.0$, beyond which they don't change.

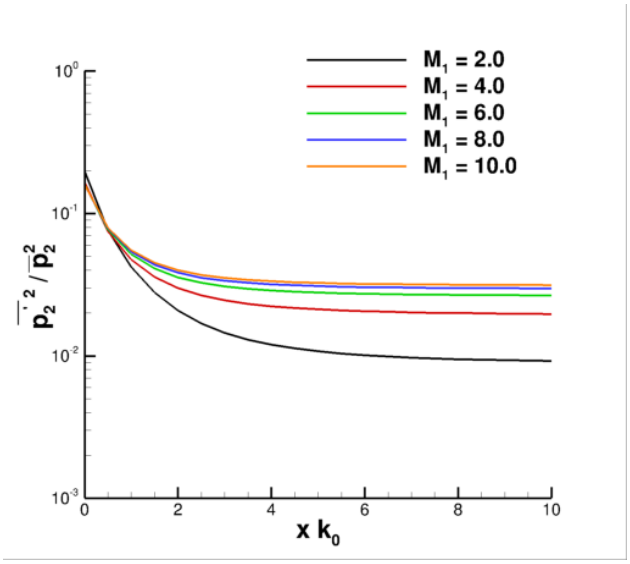


Fig. 13 Normalized variance of the downstream pressure vs. xk_0 for different upstream Mach numbers. Isotropic incident turbulence with Eqn. (63)

Figure 14 shows the three-dimensional spectra of the downstream pressure, equation (53), vs. wavenumber magnitude, normalized by the peak wavenumber, at a number of axial locations downstream of the shock, also normalized by the peak wavenumber, at Mach numbers ranging from 2.0 to 8.0 and Figure 15 shows the far-field three-dimensional spectra over the same Mach number range.

To check the effect of the functional form of the incident spectrum on the emitted pressure, Figure 16 shows results for the downstream pressure variance vs. streamwise distance downstream of the shock at various upstream Mach numbers using

$$E(k) = (k/k_0)^4 e^{-2(k/k_0)^2} \tag{64}$$

as a model for the three-dimensional spectrum of the incident turbulence. Qualitatively, these results are similar to those in Figure 13, with only the ultimate levels being lower due to the much faster high-wavenumber roll-off of (64)

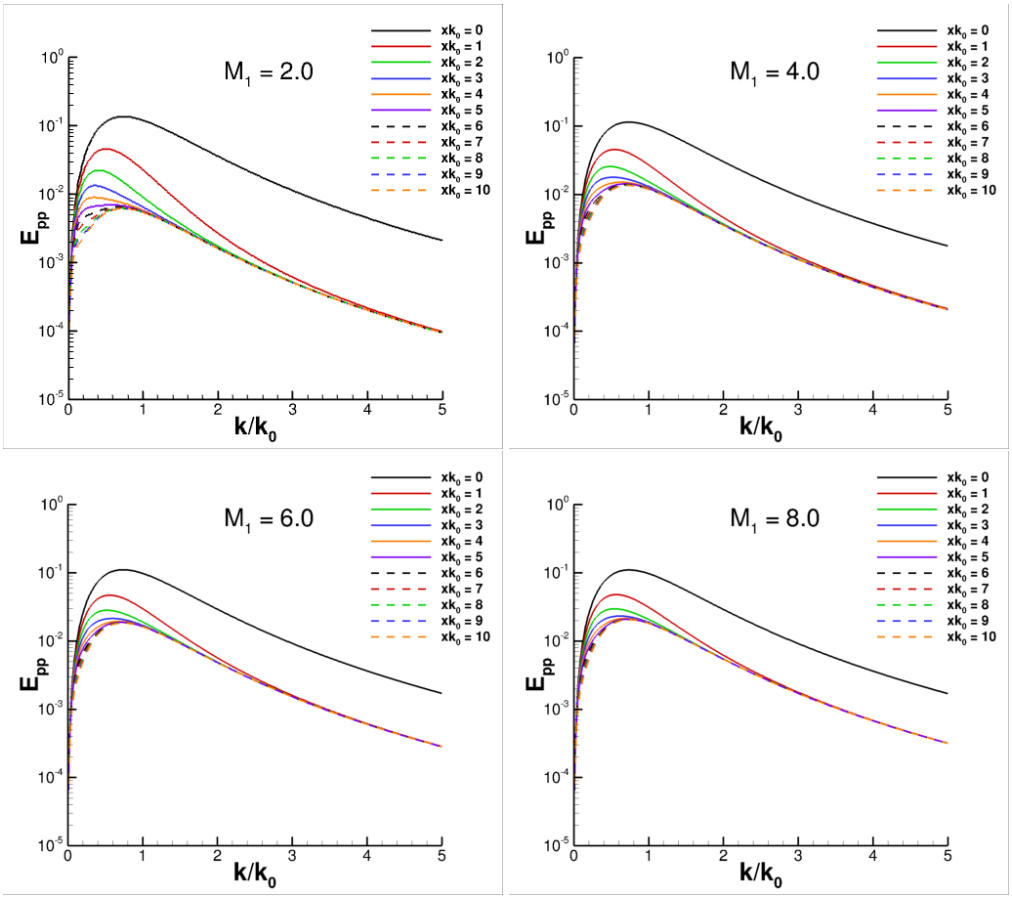


Fig. 14 Three-dimensional spectrum of the downstream pressure vs. wavenumber magnitude, normalized by the peak wave-number. Isotropic incident turbulence with Eqn (63)

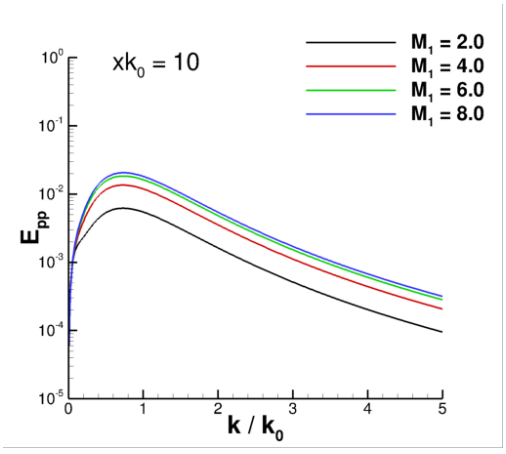


Fig. 15 Far-field three-dimensional spectrum of the downstream pressure vs. wavenumber magnitude. Isotropic incident turbulence with Eqn. (63)

compared with (63). This is also seen in the corresponding far-field three-dimension spectra of the emitted pressure using (64) shown in Figure 17.

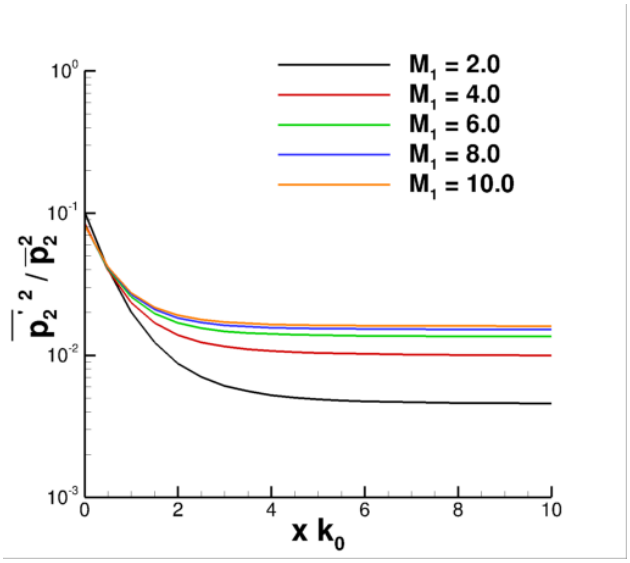


Fig. 16 Normalized variance of the downstream pressure vs. xk_0 for different upstream Mach numbers. Isotropic incident turbulence with Eqn. (64)

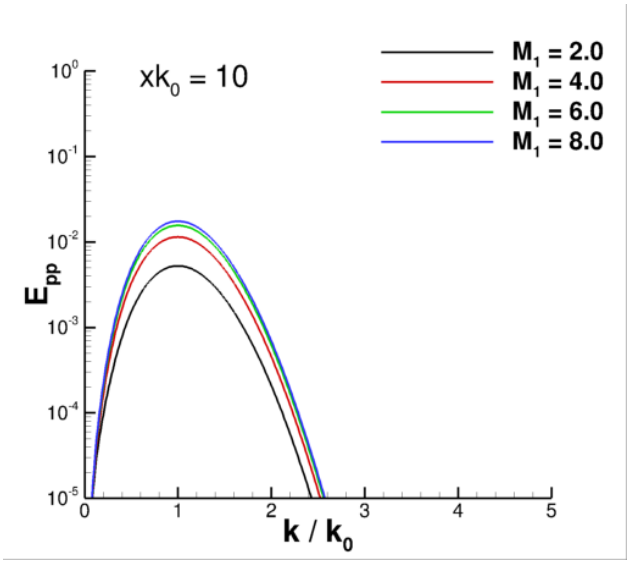


Fig. 17 Far-field three-dimensional spectrum of the downstream pressure vs. wavenumber magnitude. Isotropic incident turbulence with Eqn. (64)

C. Incident entropy mode

In this subsection we present results for an incident entropy mode, meant to represent temperature fluctuations in a heated jet. As with the results for incident vorticity mode, we first present results for individual wave components and then for an isotropic field.

1. Transfer coefficients and emitted acoustic field for single-wave components of an incident entropy mode

Figures 18 - 21 show the real and imaginary parts and the magnitudes of the transfer coefficients, $Z_{sv}, Z_{ss}, Z_{sa}, Z_{sx}$, vs. the entropy-mode-wave incident angle at upstream Mach numbers ranging from 2.0 to 8.0. In this case, the emitted entropy waves are in phase, and the vorticity, acoustic and displacement waves are out of phase, with the incident entropy waves for incident angles less than the critical value. The emitted entropy mode waves are diminished when passing through the shock, and the vorticity mode waves triggered are larger than the entropy waves generated by incident vorticity waves (Fig. 8). Amplitudes of emitted acoustic waves at small angles of incidence are higher than when a vorticity mode wave is incident, but they do not go through as large an increase near the critical angle as in the later case (see Fig. 9). This may suggest, depending on the incident spectrum, that far-field noise levels generated by incident entropy fields could be higher than that for incident vorticity fields, while the latter may result in higher amplitude noise in the vicinity of the shock.

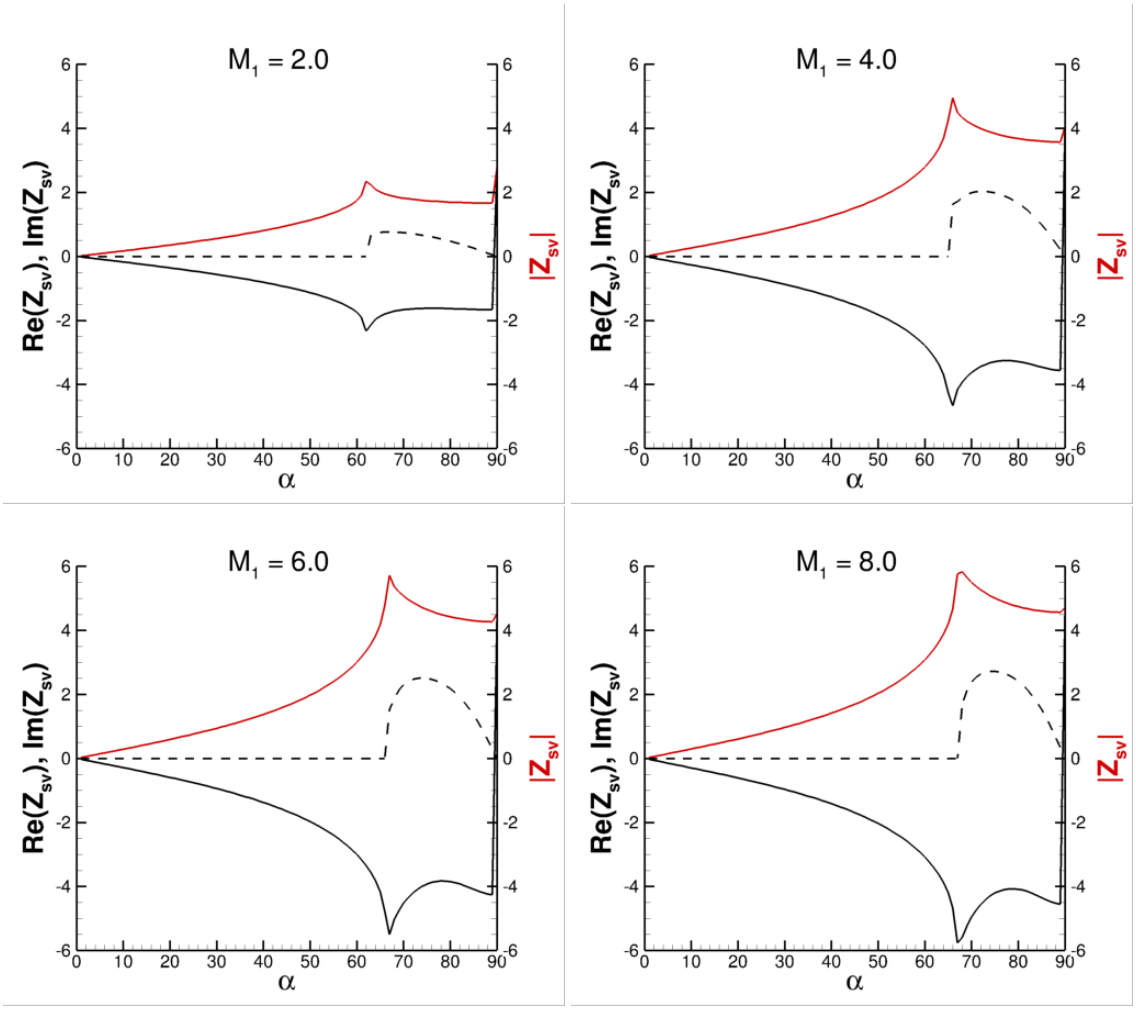


Fig. 18 Transfer coefficient for emitted Vorticity wave vs. incident Entropy mode angle; $M_1 = 2.0, 4.0, 6.0, 8.0$**. Solid black lines - Real, Dashed black lines - Imaginary and Solid red lines - Magnitude.**

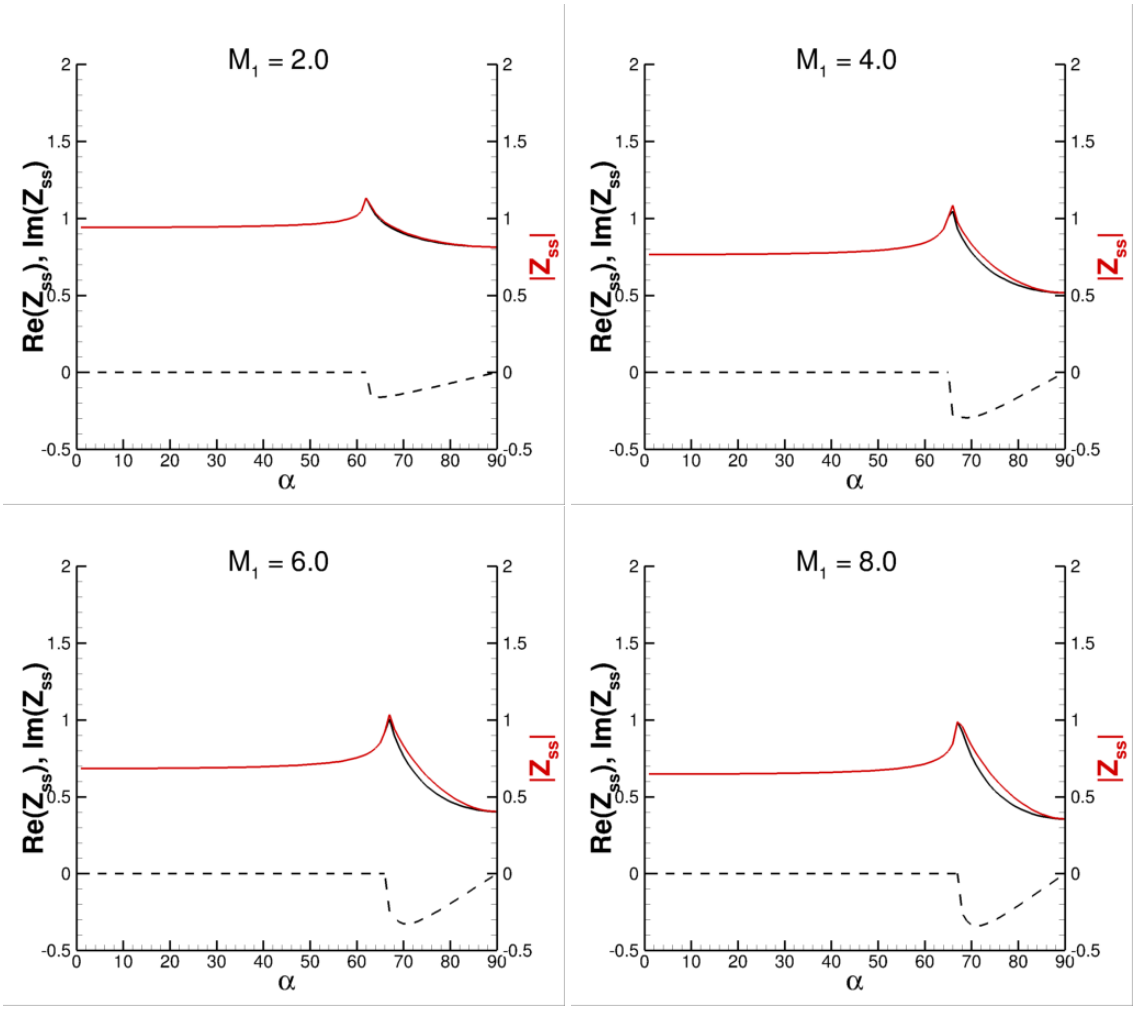


Fig. 19 Transfer coefficient for emitted Entropy wave vs. incident Entropy mode angle; $M_1 = 2.0, 4.0, 6.0, 8.0$**. Solid black lines - Real, Dashed black lines - Imaginary and Solid red lines - Magnitude.**

Figure 22 shows results for the root-mean-square (rms) amplitude of the downstream pressure, normalized by the downstream mean pressure, due to an incident single-wave entropy mode component vs. incidence angle for different streamwise locations downstream of the shock, normalized by wavenumber magnitude, for upstream Mach numbers ranging from to 2.0 to 8.0. Here also, as suggested by the results for the transfer coefficients, the emitted pressure rms undergoes a sharp increase beyond the critical angle of incidence, but lower than those for an incident vorticity mode wave (see Fig. 12). In this case also, the results become independent of upstream Mach number (or strength strength) beyond about $M_1 = 4$.

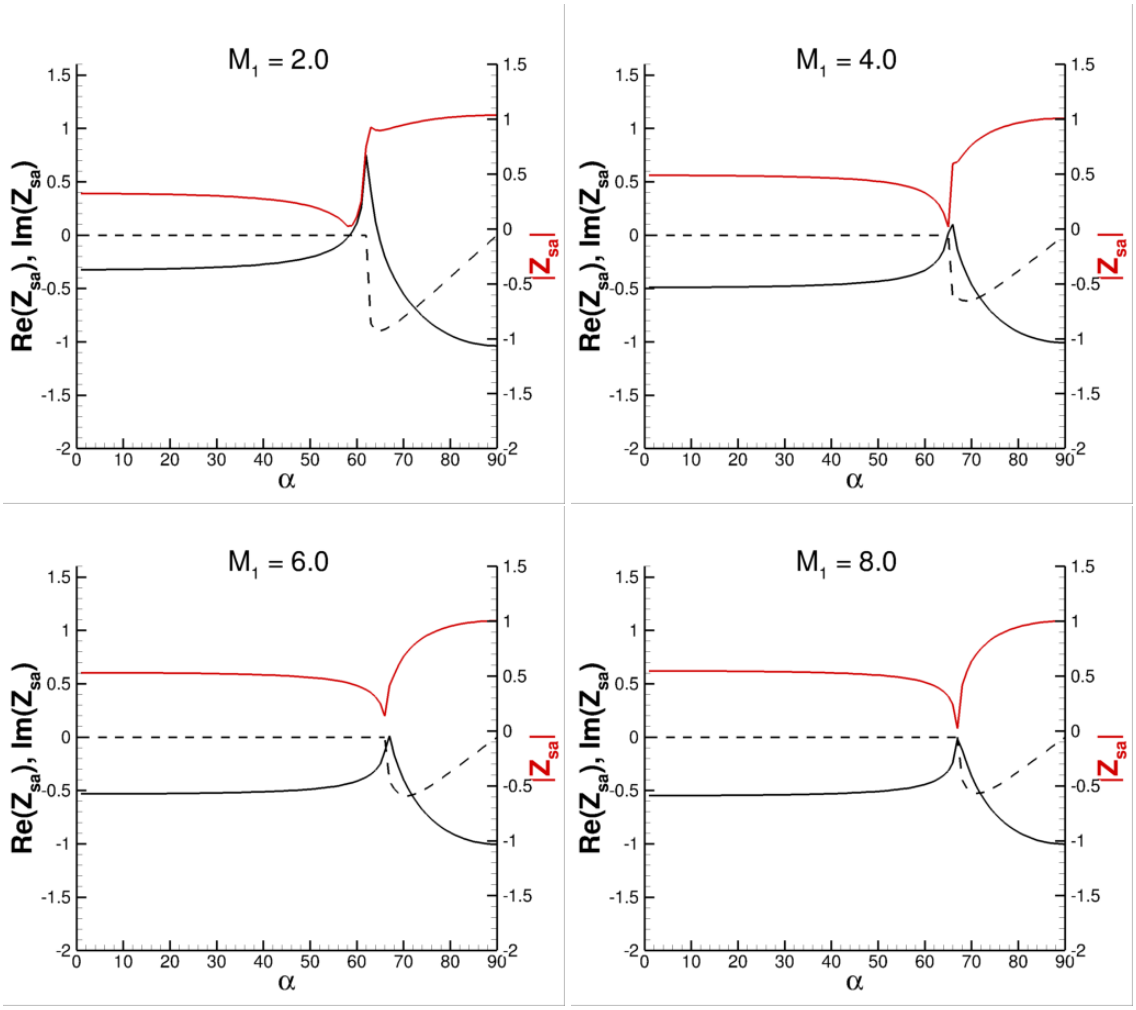


Fig. 20 Transfer coefficient for emitted Acoustic wave vs. incident Entropy mode angle; $M_1 = 2.0, 4.0, 6.0, 8.0$**. Solid black lines - Real, Dashed black lines - Imaginary and Solid red lines - Magnitude.**

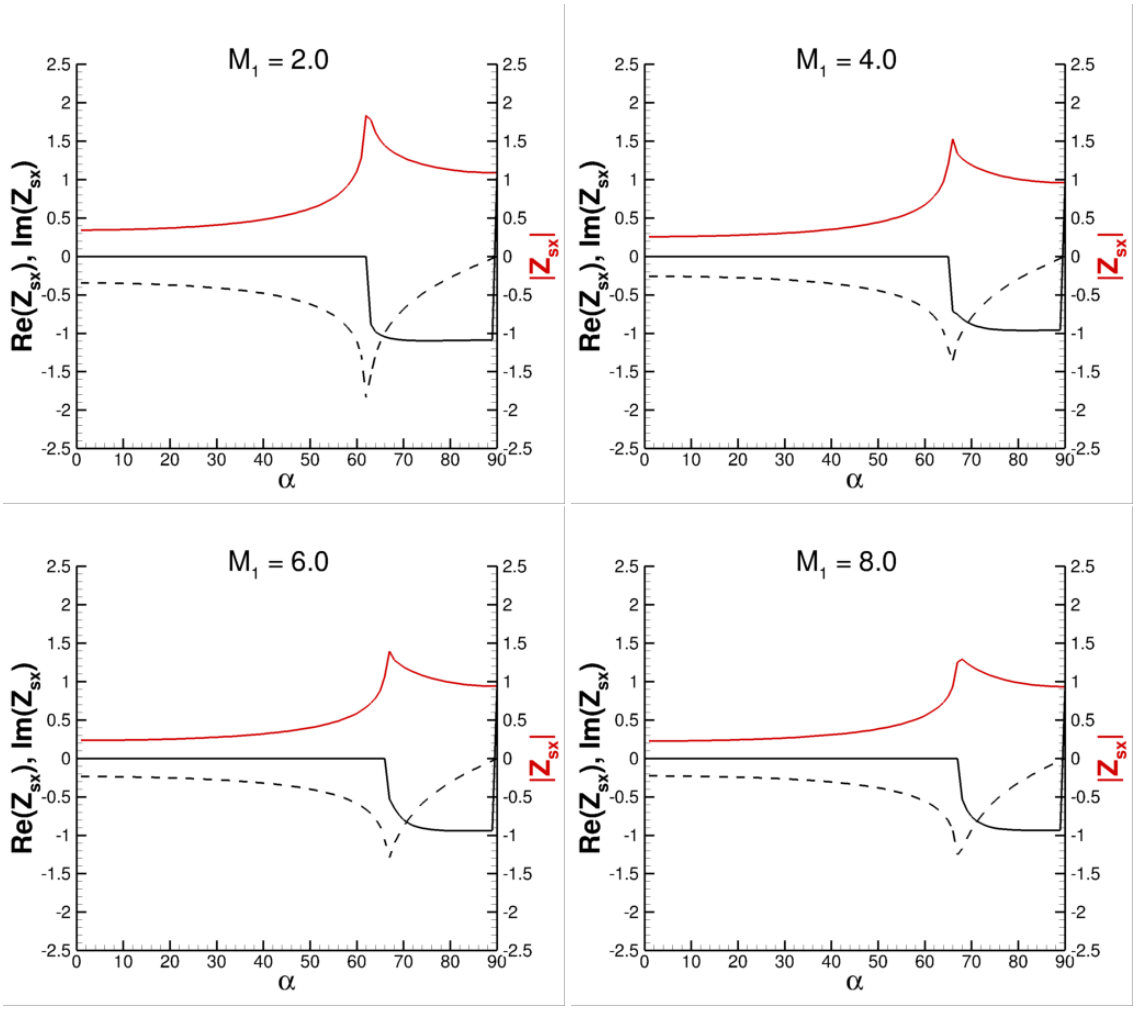


Fig. 21 Transfer coefficient for emitted Displacement wave vs. incident Entropy mode angle; $M_1 = 2.0, 4.0, 6.0, 8.0$**. Solid black lines - Real, Dashed black lines - Imaginary and Solid red lines - Magnitude.**

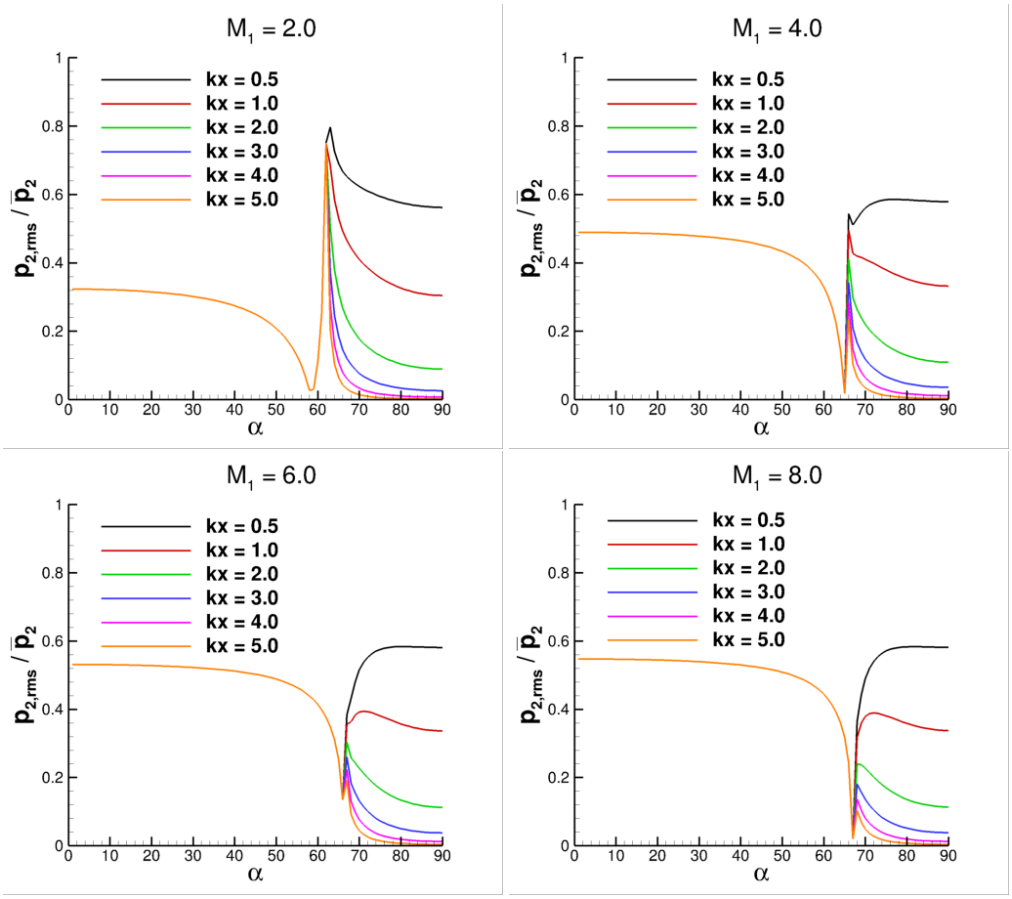


Fig. 22 Normalized root mean square amplitude of the downstream pressure for individual incident entropy mode waves vs. α for different distances downstream of the shock normalized by wavenumber magnitude for different M_1.

2. Emitted pressure field due to an incident isotropic entropy field

In this subsection we present results obtained by combining the single-wave entropy mode results of subsection V.B.1 to obtain the downstream acoustic field for an incident isotropic entropy field using the formulation in section IV

Figure 23 shows results for the normalized downstream pressure variance vs. normalized streamwise distance downstream of the shock (Eqn. (60)) at various upstream Mach numbers using the three-dimension spectrum model Eqn. (63).

Noting the different scales in Figures 13 and 23, we see that the incident distribution of entropy generates significantly higher far-field noise levels than the incident isotropic field of vortical turbulence. In contrast to the case of an incident turbulent field, the noise levels generated by the isotropic entropy field continue to increase with increasing Mach number, due to the appearance of the latter in the amplitude scaling for the entropy mode from Morkovin's hypothesis (Eqn. (57)).

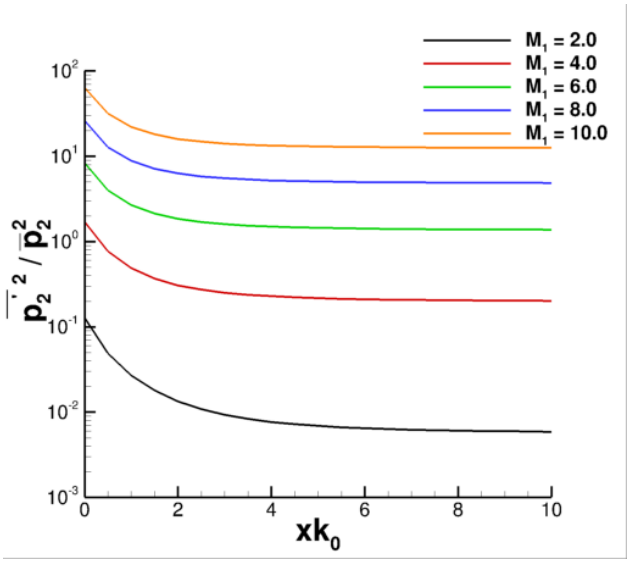


Fig. 23 Normalized variance of the downstream pressure vs. xk_0 for different upstream Mach numbers. Isotropic incident entropy field with Eqn. (63).

The corresponding three-dimensional spectra for an incident isotropic entropy field, using Eqn. (61), with Eqn. (63), are shown in Figure 24, and Figure 25 shows the far-field spectra, both for Mach numbers ranging from 2.0 to 8.0.

Figure 26 shows results for the downstream pressure variance vs. streamwise distance downstream of the shock at various upstream Mach numbers using the model three-dimensional spectrum Eqn. (64). Finally, Figure 27 show the far-field spectra using the model three-dimensional spectrum Eqn. (64).

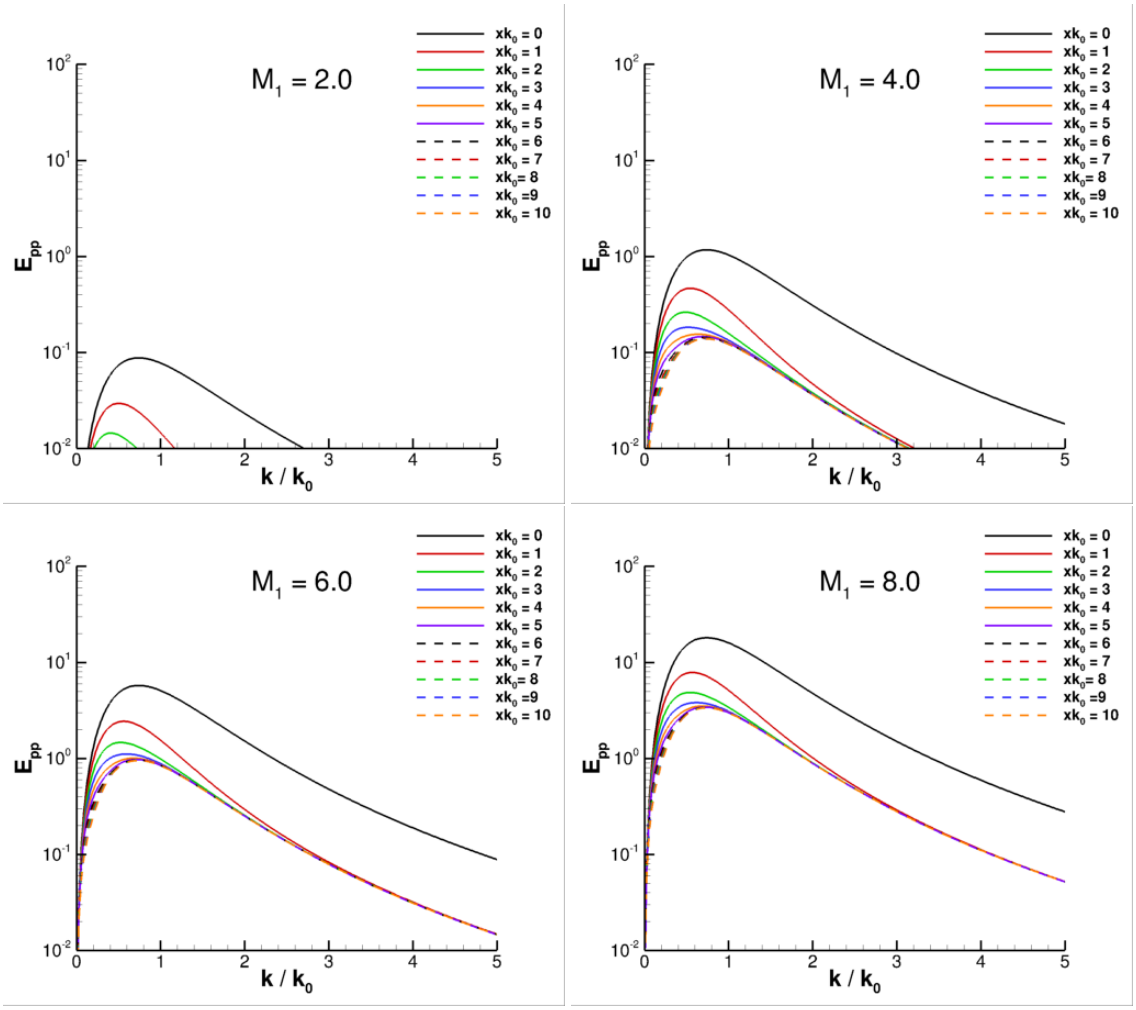


Fig. 24 Three-dimensional spectrum of the downstream pressure vs. wavenumber magnitude. Isotropic incident entropy field with Eqn. (63).

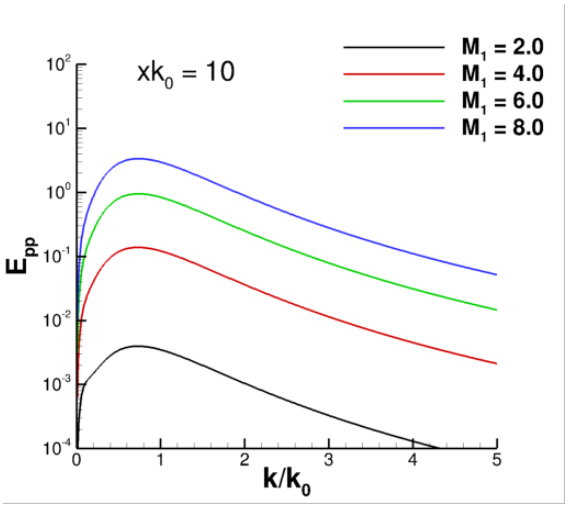


Fig. 25 Far-field three-dimensional spectrum of the downstream pressure vs. wavenumber magnitude. Isotropic incident entropy field with Eqn. (63).

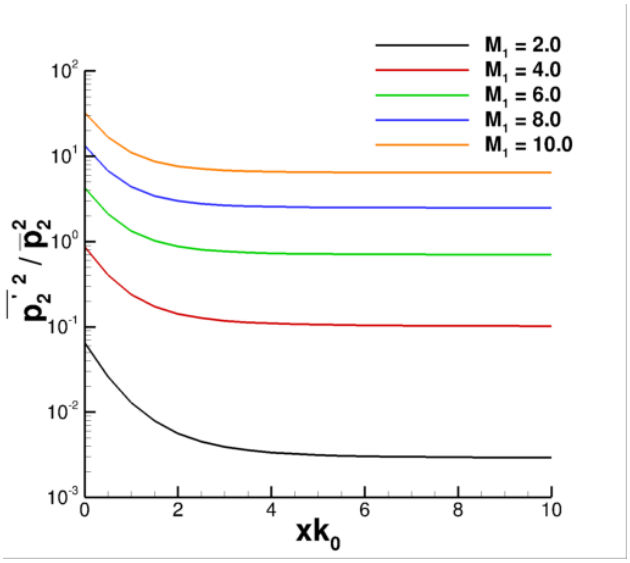


Fig. 26 Normalized variance of the downstream pressure vs. xk_0 for different upstream Mach numbers. Isotropic incident entropy field with Eqn. (64).

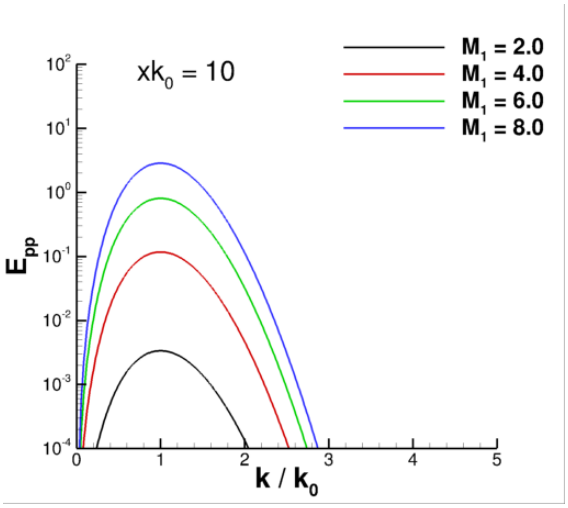


Fig. 27 Far-field three-dimensional spectrum of the downstream pressure vs. wavenumber magnitude. Isotropic incident entropy field with Eqn. (64).

VI. Summary and Future Work

In this paper we have reviewed the formulation of the Linear Interaction Approximation (LIA) and applied it to the cases of an incident vorticity and entropy mode on a planar shock, with the primary focus being on the acoustic modes generated downstream. Results for individual wave components show that incident entropy waves generate acoustic waves of larger amplitude then incident vorticity waves over most angles of incidence in the propagative regime of the former, but that in the damped regime vorticity waves produce higher levels of acoustic waves. Depending on the upstream spectral distribution, this may suggest that turbulence (vorticity modes) produces higher noise levels in the immediate vicinity of the shock, but temperature spots (entropy modes) may result in higher far-field noise levels.

The individual wave-component results were combined by integrating over all wavenumber magnitudes and incidence angles to calculate the emitted acoustic fields due to incident isotropic vorticity and entropy fields. Results are obtained using a Von Karman model for the three-dimensional spectrum of the incident turbulence and a Gaussian form. Using the Von Karman model with incident vorticity mode, at the lowest Mach number ($M = 2.0$), the variance of the downstream pressure drops by more than an order of magnitude from the shock location to the far field. At higher Mach numbers the reduction is less with the far-field levels initially increasing with increasing upstream Mach number until leveling off beyond about $M_1 = 6.0$. Similar results for the downstream pressure variance are obtained using the Gaussian spectral model but with lower levels, as expected since this spectrum drops off much faster with wavenumber magnitude.

With an isotropic entropy field incident on the shock, a similar drop off in downstream pressure variance is seen at the lowest Mach number, but both the far-field levels and those immediately behind the shock continue to increase with increasing Mach number, due to the chosen amplitude scaling of the incident entropy, Eqn. (57), which used Morkovin's hypothesis (Ref. [21]).

This work was undertaken to develop a method for assessing the noise impacts of the shock found to form at sub-critical conditions near the crown of externally plugged nozzles with internal mixers being designed for commercial supersonic aircraft. The shock is found to be a consistent feature of these exhaust configurations and its presence could alter the turbulence and sound fields passing through it in addition to being an additional noise source. In this paper we have focused on generation of noise (acoustic modes) by the (separate) incident vorticity and entropy modes on the shock. But the formulation presented here can also be used the study the change in turbulence (mixing noise sources) and (with minor extension) the scattering of upstream-generated sound when passing through the shock. The results presented in this paper demonstrate the implementation of the method on idealized incident fields. Future work will focus on applications more specific to the internally mixed and externally plugged nozzles being designed for commercial supersonic aircraft. Results from planned Large Eddy Simulations (LES) for these nozzles could be used to obtain spectral information on the turbulence upstream of the shock for use in the LIA calculations and provide data for validation of the linear predictions downstream. The impact of the shock on mixing noise could be studied by using source models from acoustic analogy formulations as incident disturbances and calculating the changes to their forms downstream of the shock. Also, by extending the formulation to include incident acoustic modes, the same general procedure can be used to study the scattering of sound produced interior to the nozzle by the mixer when it passes through the shock.

Acknowledgments

This work was supported by the NASA Advanced Air Vehicles Program, Commercial Supersonic Technology Project. The author acknowledges helpful technical discussions on this subject with Dr. James E. Bridges of NASA Glenn Research Center and thanks him for his support and for supplying the images in Figure 1.

References

[1] Bridges, J., and Wernet, M. P., "Noise of internally mixed exhaust systems with external plug for supersonic transport applications," *AIAA-2021-2218*, 2021.

[2] Bridges, J., Podboy, G. G., and Wernet, M. P., "Plug20 Test Report." *NASA/TM-2021-10291*, 2021.

[3] Tester, B. J., Fisher, M. J., and Dalton, W. N., "A contribution to the understanding and prediction of jet noise in forced mixers," *AIAA-2004-2897*, 2004.

[4] Tester, B. J., and Fisher, M. J., "A contribution to the understanding and prediction of jet noise in forced mixers: Part II Flight effects," *AIAA-2005-3094*, 2005.

[5] Tester, B. J., and Fisher, M. J., "A contribution to the understanding and prediction of jet noise in forced mixers:Part III Applications," *AIAA-2006-2542*, 2006.

[6] Garrison, L. A., Lyrintzis, A. S., Blaisdell, G. A., and Dalton, W. N., "Computational fluid dynamics analysis of jets with internal forced mixers," *AIAA-2005-2887*, 2005.

[7] Moore, F. K., "Unsteady Oblique Interaction of a Shock Wave with a Plane Disturbance," *NACA TN 2879*, 1953.

[8] Ribner, H. S., "Convection of a Pattern of Vorticity Through a Shock Wave," *NACA TN 1164*, 1954.

[9] Ribner, H. S., "Shock-Turbulence Interaction and the Generation of Noise," *NACA TN 1233*, 1955.

[10] Ribner, H. S., "Spectra of noise and amplified turbulence emanating from shock-turbulence interaction," *AIAA Journal*, Vol. 25, No. 3, 1987.

[11] Sagaut, P., and Cambon, C., *Homogeneous Turbulence Dynamics*, 2nd ed., Springer-Verlag, New York, 2018.

[12] Chang, C., "Interaction of a plane shock and oblique plane disturbances with spectial reference to entropy waves," *J. Aero. Sci.*, Vol. 24, 1957.

[13] Manesh, K., Moin, P., and Lele, S., "The interaction of a shock wave with a turbulent flow," *Tech. Report TF-69, Thermosciences Division, Department of Mechanical Engineering, Stanford University*, 1996.

[14] Manesh, K., Moin, P., and Lele, S., "The influence of entropy fluctuations on the interaction of turbulence with a shock wave," *Journal of Fluid Mechanics*, Vol. 334, 1997.

[15] Lee, S., Lele, S. K., and Moin, P., "Interaction of isotropic turbulence with shock waves: effect of shock strength," *Journal of Fluid Mechanics*, Vol. 340, 1997.

[16] Fabre, D., Jacquin, L., and Sesterhenn, J., "Linear interaction of a cylindrical entropy spot with a shock," *Physics of Fluids*, Vol. 13, No. 8, 2001.

[17] Thakare, P., Nair, V., and Sihna, K., "A weakly nonlinear framework to study shock-vorticity interaction," *Journal of Fluid Mechanics*, Vol. 933, 2022.

[18] Kovaszany, L. S. G., "Turbulence in Supersonic Flow," *J. Aero. Sci.*, Vol. 20, No. 11, 1953, pp. 657–682. https://doi.org/10.2514/3.13046.

[19] Liepmann, H. W., and Roshko, A., *Elements of Gasdynamics*, 2nd ed., John Wiley & Sons, New York, 1957.

[20] Hinze, J., *Turbulence*, 2nd ed., McGraw-Hill, New York, 1975.

[21] Morkovin, M. V., "Effects of compressibility on turbulent flows," *in Mecanique de la Turbulence (ed. A. Faver), 367-380.*, 1960.